Multi-Resolution Analysis and Upwinding for Uncertain Nonlinear Hyperbolic Systems

Julie Tryoen, Olivier Le Maitre, Michael Ndjinga, Alexandre Ern

Multi-Resolution Analysis and Upwinding for Uncertain Nonlinear Hyperbolic Systems

J. Tryoen[a,b,*], O. Le Maître[b,c], M. Ndjinga[c], A. Ern[a]

[a] *Université Paris Est, CERMICS, Ecole des Ponts, 77455 Marne la Vallée cedex 2, France*
[b] *LIMSI-CNRS, 91403 Orsay cedex, France*
[c] *CEA/Saclay/DEN/DM2S/SFME/LGLS, 91191 Gif-sur-Yvette cedex, France*

Abstract

This paper deals with spectral stochastic methods for uncertainty propagation and quantification in nonlinear hyperbolic systems of conservation laws. We consider problems with parametric uncertainty in initial conditions and model coefficients, whose solutions exhibit discontinuities in physical as well as in stochastic spaces. The spectral stochastic method relies on multi-resolution schemes with multi-wavelet or local polynomial bases. A Galerkin projection is used to derive a system of deterministic equations for the stochastic modes of the solution. Hyperbolicity of the resulting Galerkin system is analyzed. A finite volume scheme with a Roe-type solver is used for discretization in physical space and time. An original technique is introduced for the fast evaluation of approximate upwind matrices, which is particularly well adapted to local polynomial bases. Efficiency and robustness of the overall method are assessed on the Burgers and Euler equations with shocks.

Key words: Uncertainty Quantification, hyperbolic systems, conservation laws, spectral stochastic methods, Multi-Resolution, upwinding

1. Introduction

In numerical simulation, accounting for uncertainties in input quantities (such as model parameters, initial and boundary conditions, and geometry) is an important issue, especially in risk analysis, safety, and design. Assuming that these input quantities can be parametrized by random variables with known distribution functions, the question is to quantify the resulting uncertainty in the numerical solution. Uncertainty Quantification (UQ) provides for instance numerical error bars that make the comparison with experimental observations easier and therefore facilitate the evaluation of the validity of the physical models. Moreover, they enable to identify the uncertain parameters that should be measured or controlled with more accuracy because they have the most signifiant impact on the solution. Furthermore, they allow to assess the level of reliability that can be attached to computations.

Spectral stochastic methods provide effective tools for UQ. Such methods decompose random quantities on suitable approximation bases. Their main interest is that they provide a complete probabilistic description of the uncertain solution. A classical choice for the stochastic basis is the set of generalized Polynomial Chaos (gPC) spanned by random polynomials, continuous on the stochastic space and truncated to some degree. Polynomial Chaos (PC) methods were originally introduced by Ghanem and Spanos [11] following the Wiener Chaos theory [34] in which random processes are expanded in a Hermite polynomial basis of Gaussian random variables. The theory was then extended to the case of more general random processes

* *Corresponding author*: Université Paris Est, CERMICS, Ecole des Ponts, 77455 Marne la Vallée cedex 2, France. Phone: (33)-1 64 15 36 65

Email addresses: tryoen@cermics.enpc.fr (J. Tryoen), olm@limsi.fr (O. Le Maître), michael.ndjinga@cea.fr (M. Ndjinga), ern@cermics.enpc.fr (A. Ern)

that can be expanded on a basis of orthogonal polynomials associated with the chosen random variables; see among others [36]. Then, two types of resolution methods are available. The first ones are called non-intrusive and are based on the use of the numerical code solving the deterministic model (without uncertainty) as a black box to construct the spectral expansion of the solution. Two approaches can be used, either the probabilistic collocation method [25, 35, 2, 9, 29, 8], which consists in approximating the stochastic solution by a polynomial interpolation, or the non-intrusive projection method [31, 14, 22], which is based on the evaluation of the stochastic modes of the solution by numerical integration. For the two cases, the issue is to find the set of interpolation or integration points that provide the most accurate stochastic approximation. The second type of resolution methods are stochastic Galerkin methods based on a Galerkin projection of the model equations yielding a reformulated deterministic problem for the stochastic modes of the solution. Such methods are called intrusive because of the need to rewrite to some extent the simulation code. Their advantage is to rely on the weak form of the problem and thereby on a firmer theoretic background. Therefore, they are in our opinion better suited for mathematical analysis and improvements such as refinement and adaptation. In particular, stochastic Galerkin methods applied to elliptic and parabolic problems are relatively well understood. Such methods have been successfully applied in many domains (see [11] and references therein). Regarding viscous flow models, previous works have dealt with the incompressible Navier-Stokes equations [21, 22], Low Mach number flows [20], and electrochemical microfluidic applications [5]. Recent reviews on uncertain fluid flows can be found in [15, 27].

The application of spectral stochastic methods to hyperbolic systems of conservation laws (in particular inviscid flows) poses additional challenges. The main difficulty is that solutions can exhibit discontinuities (in physical space) in finite time due to the developpement of shock waves and contact discontinuities. Although these discontinuities are in physical space, their propagation speed can be affected by uncertainty, thereby leading to discontinuities in stochastic space as well. As a result, bases of continuous polynomials in the stochastic space become inappropriate, because of aliasing errors [3] and Gibbs-type phenomena [17]. To overcome this issue, Multi-Resolution Analysis (MRA) methods using stochastic finite elements [4], multi-element gPC (ME-gPC) [33], and multi-wavelet expansions [17, 18, 19] can be used to make the spectral representation more local by decomposing the stochastic space into different regions or different scales. Another difficulty originates from the nonlinearities in the physical fluxes of the stochastic hyperbolic system raising the subtle issue of computing such fluxes in the context of Galerkin projections. Indeed, all mathematical operations must be applied to the stochastic expansions that represent the variables. One attractive approach is to use pseudo-spectral techniques [6].

Polynomial collocation methods have already been applied by Mathelin et al. [26] to the Euler equations but in the continuous case. Other non-intrusive approaches include that of Abgrall [1] based on ENO-like recontructions for the convection, Burgers, and Euler equations, and that of Lin et al. [24] based on multi-element probabilistic collocation methods for supersonic flows past a wedge with random roughness. Concerning intrusive methods, most of the approaches found in the literature are in fact pseudo-intrusive because the fluxes in the Galerkin system are computed in a non-intrusive way by quadrature methods, as for instance in Ge et al. [10] for the shallow-water equations and in Poette et al. [30] for the Burgers and Euler equations. One nice feature of this latter approach is that the polynomial expansion is carried on suitable entropic variables and not on the original conservative variables, so that it can be proven that the Galerkin projection leads to a hyperbolic system; however the numerical algorithm requires a minimization procedure to recover the solution expansion that can be time consuming.

To our knowledge, very few fully intrusive spectral stochastic methods have been investigated for uncertain hyperbolic problems. The scalar wave equation has been treated with gPC methods by Gott et al. [13]. The case of nonlinear hyperbolic systems is obviously more difficult. Supersonic flows past a wedge with random inflow fluctuations or random wedge oscillations around its apex have been studied using ME-gPC methods by Lin et al. [23]. In the context of fully intrusive methods, a crucial question is the design of a suitable scheme to approximate in physical space and time the evolution problem associated with the Galerkin projection. Typically, one would like to use a Finite Volume (FV) scheme with appropriate upwinding. For instance, Lin et al. [23] considered upwinding using the mean values (in stochastic space) of the eigenvectors of the Galerkin Jacobian matrix. As mentionned in [23], this approach is only justified in the case of relatively small fluctuations of the random quantities. The present paper improves on this point

both theoretically and numerically, by using full spectral information on the eigenvectors of the Galerkin Jacobian matrix and by proposing a cost-effective method to approximate the absolute value of this matrix.

The purpose of the present work is to investigate fully intrusive MRA methods for nonlinear stochastic hyperbolic systems. To this end we choose to decompose the random space dyadically and approximate the stochastic solution on piecewise polynomial spaces. We consider two types of orthogonal bases for these spaces: the Multi-Wavelet (MW) basis [18] and the local tensorized (Legendre) polynomial basis, henceforth referred to as the Stochastic Element (SE) basis. A Stochastic Galerkin projection is then used to derive the Galerkin system, that is, the set of deterministic equations coupling the stochastic modes of the solution on the selected basis. The nonlinear fluxes in the Galerkin system are computed in a pseudo-spectral way with the tools described in [6]. At the theoretical level, our main result is that the Galerkin system is proven to be hyperbolic in two specific cases, namely when the original stochastic problem has a symmetric Jacobian and when its eigenvectors are independent of the uncertainty. Moreover, in the general case, the Galerkin Jacobian matrix is shown to be close to a $\mathbb{R}$-diagonalizable matrix. These results are independent of the choice of bases (MW or SE). Finally, a FV method with a Roe-type solver is used to approximate the Galerkin system in physical space and time. One novel feature of the proposed methodology is the fast computation of approximate upwind matrices. It consists in applying a low-degree polynomial transform to the Galerkin Jacobian matrix. This polynomial is determined only from the eigenvalues of the original stochastic problem. This approach is particularly well adapted to the SE basis since the computation of the polynomial can be localized to each stochastic element.

The paper is organized as follows. In Section 2, the stochastic hyperbolic framework is presented, including the stochastic subspaces and the stochastic Galerkin projection. The hyperbolicity of the Galerkin system is investigated in Section 3. Numerical methods are described in Section 4. Finally, simulation results are presented in Section 5.

We adopt the following notation: lower case symbols represent deterministic quantities, whereas upper case symbols represent stochastic quantities.

2. Galerkin projection of stochastic hyperbolic systems

2.1. Probabilistic framework and parametric uncertainty

We are interested in uncertainty propagation and quantification in nonlinear hyperbolic problems. The uncertainty is treated in a probabilistic framework. We rely on an abstract probability space $\mathcal{P} = (\Theta, \Sigma, \mathrm{d}\mu)$, where Θ is the set of random events, Σ the associated σ-algebra, and $\mathrm{d}\mu$ the probability measure. For any random variable $H(\theta)$ defined on $\mathcal{P}$, the expectation of H is

$$E[H] = \int_\Theta H(\theta)\mathrm{d}\mu(\theta). \tag{1}$$

We denote by $L^2(\Theta, \mathrm{d}\mu)$ the space of second-order random variables on $\mathcal{P}$. We assume hereafter that all random quantities are second-order.

Since $\mathcal{P}$ is abstract, one needs to introduce a more convenient space allowing for a stochastic discretization. This is achieved by introducing a parametrization involving a finite set of N random variables $\xi(\theta) \equiv \{\xi_1(\theta), \dots, \xi_\mathrm{N}(\theta)\}$ defined on $\mathcal{P}$ with known distributions. For simplicity, we consider $\xi_i(\theta)$ as real-valued independent identically distributed random variables, such that the joined density function of $\xi(\theta)$ factorizes, namely

$$p_\xi(y) = \prod_{i=1}^{\mathrm{N}} p(y_i), \tag{2}$$

where $p(y_i)$ is the probability density function of $\xi_i(\theta)$. We further denote by Ξ the range of ξ and by $\mathcal{P}_\xi$ the image probability space, $\mathcal{P}_\xi \equiv (\Xi, \mathcal{B}_\Xi, p_\xi)$, where $\mathcal{B}_\Xi$ is the Borel set of Ξ. Similarly, $L^2(\Xi, p_\xi)$ is the space of second-order random variables defined on the image space. The expectation operator in the image space is denoted using brackets and is related to the expectation on $\mathcal{P}$ through the identity

$$E[H] = \int_\Theta H(\xi(\theta))\mathrm{d}\mu(\theta) = \int_\Xi H(y)p_\xi(y)\mathrm{d}y \equiv \langle H \rangle . \tag{3}$$

2.2. Stochastic hyperbolic systems

We consider uncertain physical systems modelled by conservative systems of nonlinear hyperbolic PDE's. The uncertainty can result from a variability of the initial condition and/or of some coefficients in the model. For simplicity, we focus on one-dimensional problems in physical space. The extension to higher physical space dimension is straightforward at least concerning the stochastic aspects. We seek for $U(x,t,\xi)$ solving almost surely the following conservative system

$$\begin{cases} \dfrac{\partial}{\partial t}U(x,t,\xi) + \dfrac{\partial}{\partial x}F(U(x,t,\xi);\xi) = 0, \\ U(t=0,x,\xi) = U^0(x,\xi). \end{cases} \tag{4}$$

Let $\Omega \subset \mathbb{R}$ be the physical bounded domain over which the problem is posed and let $\mathcal{A}_U \subset \mathbb{R}^m$, $m \geq 1$, be the set of admissible values for the solutions of the deterministic version of (4). For instance, for the Burgers equation, we can take $\mathcal{A}_U = \mathbb{R}$, whereas for the Euler equations $\mathcal{A}_U$ is the set of states with positive density and pressure. Then, $U : (x,t,\xi) \in \Omega \times [0,T] \times \mathcal{P} \mapsto U(x,t,\xi) \in \mathcal{A}_U \otimes L^2(\Xi, p_\xi)$ denotes the uncertain state vector of conservative variables parametrized by ξ, $U^0(x,\xi)$ is a parametrization by ξ of the uncertain initial condition, and $F : (U,\xi) \in \mathcal{A}_U \otimes L^2(\Xi, p_\xi) \times \mathcal{P} \mapsto F(U;\xi) \in \mathbb{R}^m \otimes L^2(\Xi, p_\xi)$ is the uncertain flux function, involving some random coefficients parametrized again by ξ. Moreover, since the domain Ω is bounded, appropriate boundary conditions have to be enforced at the boundary $\partial\Omega$; they will be specified in Section 5 when presenting the test cases.

The system (4) can also be written in the non-conservative form

$$\begin{cases} \dfrac{\partial}{\partial t}U(x,t,\xi) + \nabla_U F(U(x,t,\xi);\xi)\dfrac{\partial}{\partial x}U(x,t,\xi) = 0, \\ U(t=0,x,\xi) = U^0(x,\xi). \end{cases} \tag{5}$$

This stochastic system is assumed to be hyperbolic in the sense that the stochastic Jacobian matrix $\nabla_U F \in \mathbb{R}^{m,m} \otimes L^2(\Xi, p_\xi)$ is $\mathbb{R}$-diagonalizable almost surely.

2.3. Stochastic discretization

To approximate the solution in $L^2(\Xi, p_\xi)$, we need a stochastic discretization of the problem. This is classically obtained by considering an appropriate Hilbertian basis of random functionals in ξ spanning $L^2(\Xi, p_\xi)$,

$$L^2(\Xi, p_\xi) = \overline{span\{\Psi_0(\xi), \Psi_1(\xi), \dots\}}, \quad \langle \Psi_\alpha \Psi_\beta \rangle = \delta_{\alpha\beta}, \tag{6}$$

where $\delta_{\alpha\beta}$ denotes the Kronecker symbol. The discrete solution is sought in a finite dimensional subspace $\mathcal{S}^{\mathrm{P}}$ constructed by truncating the Hilbertian basis:

$$\mathcal{S}^{\mathrm{P}} = span\{\Psi_0(\xi), \Psi_1(\xi), \dots, \Psi_{\mathrm{P}}(\xi)\} \subset L^2(\Xi, p_\xi), \quad \dim(\mathcal{S}^{\mathrm{P}}) = \mathrm{P}+1. \tag{7}$$

We assume for simplicity that ξ is a uniform random vector in $[0,1]^{\mathrm{N}}$ (an isoprobabilistic transformation can be used to map the original independent random variables to this random vector). The image probability space is then $\mathcal{P}_\xi \equiv ([0,1]^{\mathrm{N}}, \mathcal{B}_{[0,1]^{\mathrm{N}}}, 1)$, where $\mathcal{B}_{[0,1]^{\mathrm{N}}}$ is the Borel set of $[0,1]^{\mathrm{N}}$.

We adopt a multi-resolution approach by decomposing the random domain dyadically and approximating the stochastic solution by piecewise polynomial functions. In addition to the number N of random variables ξ_i in the parametrization, this approximation depends on the resolution level $\mathrm{Nr} \geq 0$ (controlling the minimal size of the stochastic elements, that is, the discretization cells in the stochastic space) and on the expansion order $\mathrm{No} \geq 0$ (controlling the degree of the piecewise polynomial approximation). Let $\mathtt{i} = (i_1, \dots, i_{\mathrm{N}}) \in \{1, \dots, 2^{\mathrm{Nr}}\}^{\mathrm{N}}$ be a multi-index and let $K_{\mathtt{i}} = \{\xi \in [0,1]^{\mathrm{N}}, \forall 1 \leq j \leq \mathrm{N}, \xi_j \in]2^{-\mathrm{Nr}}(i_j-1), 2^{-\mathrm{Nr}} i_j[\}$ be the associated stochastic element. Thus, we define $\mathcal{S}^{\mathrm{No,Nr}}$ as the stochastic approximation space of piecewise polynomial functions

$$\mathcal{S}^{\mathrm{No,Nr}} = \{f : [0,1]^{\mathrm{N}} \to \mathbb{R}, \forall \mathtt{i} \in \{1, \dots, 2^{\mathrm{Nr}}\}^{\mathrm{N}}, f|_{K_{\mathtt{i}}} \in \mathbb{Q}^{\mathrm{N}}_{\mathrm{No}}[\xi]\}, \tag{8}$$

where $\mathbb{Q}_{\mathrm{No}}^{\mathrm{N}}[\xi]$ denotes the vector space of real polynomials in $\mathbb{R}^{\mathrm{N}}$ with degree $\leq \mathrm{No}$ in each variable ξ_i. The space $\mathcal{S}^{\mathrm{No,Nr}}$ has dimension

$$\dim \mathcal{S}^{\mathrm{No,Nr}} = (\mathrm{No}+1)^{\mathrm{N}} 2^{\mathrm{N}\mathrm{Nr}} = \mathrm{P}+1. \tag{9}$$

Observe that the spaces $\mathcal{S}^{\mathrm{No,Nr}}$ form a hierarchical family of stochastic spaces since $\mathcal{S}^{\mathrm{No,Nr}} \subset \mathcal{S}^{\mathrm{No}',\mathrm{Nr}}$ for $\mathrm{No} \leq \mathrm{No}'$ and $\mathcal{S}^{\mathrm{No,Nr}} \subset \mathcal{S}^{\mathrm{No,Nr}'}$ for $\mathrm{Nr} \leq \mathrm{Nr}'$.

Two kinds of basis can be considered. Firstly, $\mathcal{S}^{\mathrm{No,Nr}}$ can be spanned by the hierarchical Multi-Wavelet system of order No and resolution level Nr introduced in [18]. This yields the Multi-Wavelet (MW) basis $\{\psi_\alpha^{MW}(\xi)\}_{\alpha=0,\ldots,\mathrm{P}}$. Alternatively, $\mathcal{S}^{\mathrm{No,Nr}}$ can be spanned by local Legendre polynomial bases, where each function of $\mathcal{S}^{\mathrm{No,Nr}}$ is expanded in each stochastic element of size $2^{-\mathrm{Nr}}$ on a local fully tensorized set with dimension $(\mathrm{No}+1)^{\mathrm{N}}$ of Legendre polynomials. For convenience, Legendre polynomials are henceforth defined with respect to the reference interval $[0,1]$. This yields the Stochastic Element (SE) basis $\{\psi_\alpha^{SE}\}_{\alpha=0,\ldots,\mathrm{P}}$. The case $\mathrm{Nr}=0$ corresponds to the classical continuous approximation (Wiener-Legendre expansion), while the choice $\mathrm{Nr}>0$ and $\mathrm{No}=0$ leads to the Wiener-Haar expansion (piecewise constant approximation). For further use, let $B \in \mathbb{R}^{\mathrm{P}+1,\mathrm{P}+1}$ denote the transition matrix between the two bases, such that $\Psi_\alpha^{MW}(\xi) = \sum_{\gamma=0}^{\mathrm{P}} B_{\alpha\gamma}\Psi_\gamma^{SE}(\xi)$, for all $\alpha = 0,\ldots,\mathrm{P}$.

The approximate solution in $\mathcal{S}^{\mathrm{P}} := \mathcal{S}^{\mathrm{No,Nr}}$ is expanded as a series in the form

$$U(x,t,\xi) \approx U^{\mathrm{P}}(x,t,\xi) = \sum_{\alpha=0}^{\mathrm{P}} u_\alpha(x,t)\Psi_\alpha(\xi). \tag{10}$$

The deterministic $\mathbb{R}^m$-valued fields $u_\alpha(x,t)$ are called the stochastic modes of the solution (in $\mathcal{S}^{\mathrm{P}}$). If $U^{\mathrm{P}}(x,t,\xi)$ is known, then $u_\alpha = \langle \Psi_\alpha U^{\mathrm{P}} \rangle$. The basis functions Ψ_α are either Ψ_α^{MW} or Ψ_α^{SE} defined above. Let u_α^{MW} and u_α^{SE} denote the stochastic modes expressed in the two different bases. Then, $u_\alpha^{MW} = \sum_{\gamma=0}^{\mathrm{P}} B_{\alpha\gamma} u_\gamma^{SE}$, for all $\alpha = 0,\ldots,\mathrm{P}$.

2.4. The Galerkin problem

The computation of the stochastic modes $u_\alpha(x,t)$ is based on a weak interpretation, or Galerkin projection, of (4). Projecting (4) on the basis of $\mathcal{S}^{\mathrm{P}}$, we obtain

$$\begin{cases} \left\langle \Psi_\alpha \dfrac{\partial U^{\mathrm{P}}}{\partial t} \right\rangle + \left\langle \Psi_\alpha \dfrac{\partial F(U^{\mathrm{P}};\cdot)}{\partial x} \right\rangle = 0, & \forall \alpha = 0,\ldots,\mathrm{P}, \\ \left\langle \Psi_\alpha U^{\mathrm{P}} \right\rangle (t=0) = \left\langle \Psi_\alpha U^0 \right\rangle, & \forall \alpha = 0,\ldots,\mathrm{P}. \end{cases} \tag{11}$$

Accounting for orthonormality, (11) is equivalent to

$$\begin{cases} \dfrac{\partial}{\partial t} u_\alpha(x,t) + \dfrac{\partial}{\partial x} \left\langle \Psi_\alpha F\left(U^{\mathrm{P}};\cdot\right) \right\rangle = 0, & \forall \alpha = 0,\ldots,\mathrm{P}, \\ u_\alpha(x,t=0) = \left\langle \Psi_\alpha U^0 \right\rangle, & \forall \alpha = 0,\ldots,\mathrm{P}. \end{cases} \tag{12}$$

Equation (12) shows that the α-th stochastic mode of the approximate solution is governed by an equation that generally couples all the stochastic modes in the term $\langle \Psi_\alpha F(U^{\mathrm{P}};\cdot) \rangle$. It is convenient to define the vectors of stochastic modes and flux

$$u(x,t) = \begin{pmatrix} u_0(x,t) \\ \vdots \\ u_{\mathrm{P}}(x,t) \end{pmatrix}, \qquad f(u(x,t)) = \begin{pmatrix} f_0(u) \\ \vdots \\ f_{\mathrm{P}}(u) \end{pmatrix}, \tag{13}$$

with

$$f_\alpha(u) \equiv \left\langle \Psi_\alpha F\left(U^{\mathrm{P}};\cdot\right) \right\rangle, \quad \alpha = 0,\ldots,\mathrm{P}, \quad \text{and} \quad U^{\mathrm{P}} = \sum_{\beta=0}^{\mathrm{P}} u_\beta \Psi_\beta(\xi). \tag{14}$$

The component vector u must belong to the admissible set $\mathcal{A}_u \subset \mathbb{R}^{m(\mathrm{P}+1)}$ such that $u \in \mathcal{A}_u \Leftrightarrow U^{\mathrm{P}}(x,t,\xi) = \sum_{\alpha=0}^{\mathrm{P}} u_\alpha \Psi_\alpha(\xi) \in \mathcal{A}_U \otimes L^2(\Xi, p_\xi)$. With this notation, the deterministic Galerkin system takes the simple form

$$\begin{cases} \dfrac{\partial}{\partial t} u(x,t) + \dfrac{\partial}{\partial x} f(u(x,t)) = 0, \\ u(x,t=0) = u^0(x). \end{cases} \tag{15}$$

Thus, the problem on u has the same form as the original stochastic problem (4), except that the state vector is now of size $m(\mathrm{P}+1)$. The similarity of the Galerkin system (15) with (4) is a classical feature of the Galerkin projection. This similarity does not imply equivalent or comparable complexity.

The knowledge of the stochastic modes of the uncertain solution allows to compute interesting statistic quantities. For instance, in the case of the MW basis and if the convention $\Psi_0^{MW} = 1$ is adopted, the expectation of the solution is approximated by the mode $\alpha = 0$ of the expansion since

$$E[U] \approx E[U^{\mathrm{P}}] = \left\langle \sum_{\alpha=0}^{\mathrm{P}} u_\alpha^{MW} \Psi_\alpha^{MW} \right\rangle = \sum_{\alpha=0}^{\mathrm{P}} u_\alpha^{MW} \left\langle \Psi_0^{MW} \Psi_\alpha^{MW} \right\rangle = u_0^{MW}. \tag{16}$$

Similarly, the variance of the solution is given by

$$\begin{aligned} V[U] = E\left[(U - E[U])^2\right] \approx V[U^{\mathrm{P}}] = E\left[\left(U^{\mathrm{P}} - E[U^{\mathrm{P}}]\right)^2\right] &= \left\langle \left(\sum_{\alpha=1}^{\mathrm{P}} u_\alpha^{MW} \Psi_\alpha^{MW} \right)^2 \right\rangle \\ &= \sum_{\alpha,\beta=1}^{\mathrm{P}} u_\alpha^{MW} u_\beta^{MW} \left\langle \Psi_\alpha^{MW} \Psi_\beta^{MW} \right\rangle = \sum_{\alpha=1}^{\mathrm{P}} (u_\alpha^{MW})^2, \end{aligned} \tag{17}$$

where the (x,t) dependence of the solution has been dropped for simplicity. Also, once $U^{\mathrm{P}}(x,t,\xi)$ is known, one can estime various properties of the uncertain solution, such as moments, density functions, cross correlations, etc..., relying for instance on a sampling of ξ.

3. Hyperbolicity of the Galerkin system

Before detailing the construction of a numerical method to approximate the Galerkin system (15) in physical space and time, we address the issue whether this system is hyperbolic. Equation (15) can be rewritten in the non-conservative form

$$\begin{cases} \dfrac{\partial u}{\partial t} + \nabla_u f(u) \dfrac{\partial u}{\partial x} = 0, \\ u(x,t=0) = u^0(x), \end{cases} \tag{18}$$

where the Galerkin Jacobian matrix of order $m(\mathrm{P}+1)$ has a block structure such that

$$\left(\nabla_u f(u)\right)_{\alpha,\beta=0,\ldots,\mathrm{P}} = \left\langle \nabla_U F(U^{\mathrm{P}};\cdot) \Psi_\alpha \Psi_\beta \right\rangle_{\alpha,\beta=0,\ldots,\mathrm{P}}. \tag{19}$$

We aim at understanding whether the Galerkin Jacobian matrix defined by (19) is $\mathbb{R}$-diagonalizable.

An important remark is that the two different representations of $\nabla_u f$ using the MW basis or the SE basis for the stochastic discretization are equivalent in this context. Indeed, let $\nabla_u f^{MW}$ and $\nabla_u f^{SE} \in \mathbb{R}^{m(\mathrm{P}+1),m(\mathrm{P}+1)}$ be the representations of the Galerkin Jacobian matrix using each respective basis. Then, for all $\alpha, \beta = 0, \ldots, \mathrm{P}$,

$$\begin{aligned} (\nabla_u f^{MW})_{\alpha\beta} = \left\langle \nabla_U F(U^{\mathrm{P}};\cdot) \Psi_\alpha^{MW} \Psi_\beta^{MW} \right\rangle &= \sum_{\gamma,\delta} \left\langle \nabla_U F(U^{\mathrm{P}};\cdot) B_{\alpha\gamma} \Psi_\gamma^{SE} B_{\beta\delta} \Psi_\delta^{SE} \right\rangle \\ &= \sum_{\gamma,\delta} B_{\alpha\gamma} (\nabla_u f^{SE})_{\gamma\delta} B_{\beta\delta} = (B \nabla_u f^{SE} B^T)_{\alpha\beta}. \end{aligned} \tag{20}$$

Moreover, B is orthogonal owing to the orthonormality of the two bases, which implies that $\nabla_u f^{MW}$ and $\nabla_u f^{SE}$ are similar and therefore proves the equivalence of the two representations with respect to $\mathbb{R}$-diagonalization.

An advantage of using SE bases is that the Galerkin Jacobian matrix $\nabla_u f \equiv \nabla_u f^{SE}$ has a diagonal block structure, provided that the matrix coefficients are ordered according to the 2^{NNr} stochastic elements, since $(\nabla_u f)_{\alpha\beta} = 0$ whenever $Supp(\Psi_\alpha^{SE}) \cap Supp(\Psi_\beta^{SE})$ has zero measure. Consequently, $\nabla_u f$ is diagonalizable if and only if each block in the diagonal is diagonalizable. Suchs blocks are of size $m(\mathrm{No}+1)^{\mathrm{N}} \times m(\mathrm{No}+1)^{\mathrm{N}}$ and correspond to a given stochastic element. The issue of the hyperbolicity of the Galerkin system can then be studied for the case $\mathrm{Nr} = 0$.

Consider the stochastic approximation space $\mathcal{S}^{\mathrm{No},0}$, which corresponds to a Wiener-Legendre expansion of the solution. Since the stochastic Jacobian matrix $\nabla_U F(\cdot;\xi) \in \mathbb{R}^{m,m} \otimes L^2(\Xi, p_\xi)$ is $\mathbb{R}$-diagonalizable for almost every $\xi \in \Xi$, there exist m eigenvalues $\Lambda^1(\xi), \ldots, \Lambda^m(\xi)$ and m associated eigenvectors $W^1(\xi), \ldots, W^m(\xi)$ such that

$$\nabla_U F(\cdot;\xi) = P^{-1}(\xi) D(\xi) P(\xi), \tag{21}$$

with

$$D(\xi) = diag(\Lambda^k(\xi))_{k=1,\ldots,m} \quad \text{and} \quad P(\xi) = \begin{pmatrix} W^1(\xi) & \ldots & W^m(\xi) \end{pmatrix}. \tag{22}$$

The matrices $D(\xi)$ and $P(\xi)$ are in $\mathbb{R}^{m,m} \otimes L^2(\Xi, p_\xi)$.

3.1. Stochastic symmetric hyperbolic systems

Theorem 1. *If the stochastic Jacobian matrix $\nabla_U F(\cdot;\xi)$ is symmetric, then the Galerkin Jacobian matrix $\nabla_u f$ is $\mathbb{R}$-diagonalizable. In particular, the Galerkin projection of a scalar conservation law always leads to a hyperbolic system.*

Proof. If $\nabla_U F(\cdot;\xi)$ is symmetric, then the Galerkin matrix $\nabla_u f$ defined by (19) is also symmetric and therefore $\mathbb{R}$-diagonalizable. □

3.2. Stochastic eigenvectors independent of the uncertainty

Theorem 2. *If the eigenvectors of the stochastic Jacobian matrix $\nabla_U F(\cdot;\xi)$ are independent of the uncertainty, then the Galerkin Jacobian matrix $\nabla_u f$ is $\mathbb{R}$-diagonalizable.*

Proof. If the eigenvectors of $\nabla_U F(\cdot;\xi)$ are independent of ξ, then the spectral decomposition (21) becomes

$$\nabla_U F(\cdot;\xi) = p_0^{-1} D(\xi) p_0, \tag{23}$$

with

$$D(\xi) = diag(\Lambda^k(\xi))_{k=1,\ldots,m} \quad \text{and} \quad p_0 = \begin{pmatrix} w_0^1 & \ldots & w_0^m \end{pmatrix}, \tag{24}$$

where $w_0^1, \ldots, w_0^m$ are independent of ξ. A generic element in $\nabla_u f$ can be identified with the multi-index $(\alpha i, \beta j)$ with $i, j = 1, \ldots, m$ and $\alpha, \beta = 0, \ldots, \mathrm{P}$, in such a way that

$$\begin{aligned}
(\nabla_u f(u))_{\alpha i,\beta j} &= \left\langle \left(\nabla_U F(U^{\mathrm{P}};\cdot)\right)_{ij} \Psi_\alpha \Psi_\beta \right\rangle = \sum_k \left\langle \left(p_0^{-1}\right)_{ik} \Lambda^k \left(p_0\right)_{kj} \Psi_\alpha \Psi_\beta \right\rangle \\
&= \sum_k \left(p_0^{-1}\right)_{ik} \left\langle \Lambda^k \Psi_\alpha \Psi_\beta \right\rangle \left(p_0\right)_{kj} \\
&= \sum_{k,k'} \sum_{\gamma,\gamma'} \{\delta_{\alpha\gamma} \left(p_0^{-1}\right)_{ik}\} \{\delta_{kk'} \left\langle \Lambda^k \Psi_\gamma \Psi_{\gamma'} \right\rangle\} \{\delta_{\gamma'\beta} \left(p_0\right)_{k'j}\} \\
&= \sum_{k,k'} \sum_{\gamma,\gamma'} (q)_{\alpha i,\gamma k} (d)_{\gamma k,\gamma' k'} (r)_{\gamma' k',\beta j} = (q\ d\ r)_{\alpha i,\beta j}
\end{aligned} \tag{25}$$

where d is the block-diagonal matrix of size $m(\mathrm{P}+1) \times m(\mathrm{P}+1)$ such that

$$(d)_{\gamma k,\gamma' k'} = \delta_{kk'} \left\langle \Lambda^k \Psi_\gamma \Psi_{\gamma'} \right\rangle, \tag{26}$$

and q and r are $m(\mathrm{P}+1)\times m(\mathrm{P}+1)$ matrices such that

$$(q)_{\alpha i,\gamma k}=\delta_{\alpha\gamma}\left(p_0^{-1}\right)_{ik},\quad (r)_{\gamma k,\beta j}=\delta_{\gamma\beta}\left(p_0\right)_{kj}. \tag{27}$$

Each block of the diagonal of d is symmetric, and therefore $\mathbb{R}$-diagonalizable so that d is $\mathbb{R}$-diagonalizable. Besides,

$$(qr)_{\alpha i,\beta j}=\sum_{\alpha,k}(q)_{\alpha i,\gamma k}\,(r)_{\gamma k,\beta j}=\sum_{\alpha,k}\left(P_0^{-1}\right)_{ik}\delta_{\alpha\gamma}\delta_{\gamma\beta}\left(P_0\right)_{kj}=\delta_{\alpha\beta}\delta_{ij}, \tag{28}$$

which means that $q=r^{-1}$. This concludes the proof. □

Remark. Theorem 2 provides another proof of the fact that the Galerkin system derived from a stochastic scalar conservation law is hyperbolic. Indeed, $W(\xi)=1$ is the eigenvector of $\nabla_U F\in\mathbb{R}$. An application of Theorem 2 is the scalar wave equation with uncertain sound velocity.

3.3. An approximate Galerkin Jacobian matrix

In the most general case we cannot prove that the Galerkin system (15) is hyperbolic. However, we show that the Galerkin Jacobian matrix $\nabla_u f$ close to a $\mathbb{R}$-diagonalizable matrix. To show this, we consider the one-dimensional stochastic case ($\mathrm{N}=1$) and we first treat the case $\mathrm{Nr}=0$. Let $\{\xi_\gamma\}_{\gamma=0,\dots,\mathrm{No}}$ be the set of $\mathrm{P}+1=\mathrm{No}+1$ Gauss points in $[0,1]$, i.e. the $\mathrm{No}+1$ zeroes of the Legendre polynomial of degree $\mathrm{No}+1$, and let $\{\omega_\gamma\}_{\gamma=0,\dots,\mathrm{No}}$ be the associated quadrature weights.

Theorem 3. *Assume that the stochastic Jacobian matrix $\nabla_U F(\cdot;\xi)$ is defined on the $\mathrm{No}+1$ Gauss points in $[0,1]$. Consider the matrix $\overline{\nabla_u f}$ obtained by approaching the coefficients of the Galerkin Jacobian matrix $\nabla_u f$ by the above Gauss quadrature, namely*

$$\left(\overline{\nabla_u f}(u)\right)_{\alpha,\beta=0,\dots,\mathrm{No}}=\left(\sum_{\gamma=0}^{\mathrm{No}}\omega_\gamma\nabla_U F(U^{\mathrm{P}}(\xi_\gamma);\xi_\gamma)\Psi_\alpha(\xi_\gamma)\Psi_\beta(\xi_\gamma)\right)_{\alpha,\beta=0,\dots,\mathrm{No}}. \tag{29}$$

Then, $\overline{\nabla_u f}$ is $\mathbb{R}$-diagonalizable with eigenvalues $\{\Lambda^k(\xi_\eta)\}_{k=1,\dots,m,\eta=0,\dots,\mathrm{No}}$, and eigenvectors $\{v_\eta^k\}_{k=1,\dots,m,\eta=0,\dots,\mathrm{No}}$ defined by

$$\left(v_\eta^k\right)_{\beta=0,\dots,P}=\left\langle V_\eta^k\Psi_\beta\right\rangle_{\beta=0,\dots,\mathrm{No}}, \tag{30}$$

where $V_\eta^k(\xi)\in\mathbb{R}^m\otimes\mathcal{S}^{\mathrm{P}}$ is the polynomial of degree $\leq\mathrm{No}+1$ in ξ such that

$$V_\eta^k(\xi_{\eta'})=\delta_{\eta\eta'}W^k(\xi_\eta),\quad \eta'=0,\dots,\mathrm{No}. \tag{31}$$

Here, $\{\Lambda^k(\xi)\}_{k=1,\dots,m}$ and $\{W^k(\xi)\}_{k=1,\dots,m}$ are the eigenvalues and eigenvectors ot the stochastic Jacobian matrix $\nabla_U F(\cdot;\xi)$ defined in (22).

Remark. Observe that $\sum_{\eta=0}^{\mathrm{No}}V_\eta^k(\xi)$ is the interpolation polynomial of $W^k(\xi)$ at the $\mathrm{No}+1$ Gauss points.

Proof. Since the order of the quadrature is $2\mathrm{No}+1$, for all $V(\xi)\in\mathcal{S}^{\mathrm{P}}$, $\langle\Psi_\beta V\rangle$ is exact for all $\beta=0,\dots,\mathrm{No}$ if evaluated using the quadrature. Hence, for all $\beta=0,\dots,\mathrm{No}$,

$$\left(v_\eta^k\right)_\beta=\left\langle\Psi_\beta V_\eta^k\right\rangle=\sum_{\gamma=0}^{\mathrm{No}}\omega_\gamma V_\eta^k(\xi_\gamma)\Psi_\beta(\xi_\gamma)=\omega_\eta W^k(\xi_\eta)\Psi_\beta(\xi_\eta). \tag{32}$$

Furthermore, observe that for all ξ,

$$\sum_{\beta=0}^{\mathrm{No}}\left(v_\eta^k\right)_\beta\Psi_\beta(\xi)=V_\eta^k(\xi), \tag{33}$$

since the basis is orthonormal. As a result,

$$\begin{aligned}\left(\overline{\nabla_u f}(u)v_\eta^k\right)_\alpha &= \sum_{\beta=0}^{\mathrm{No}}\left(\sum_{\gamma=0}^{\mathrm{No}}\omega_\gamma \nabla_U F(U^{\mathrm{P}}(\xi_\gamma);\xi_\gamma)\Psi_\alpha(\xi_\gamma)\Psi_\beta(\xi_\gamma)\right)\left(v_\eta^k\right)_\beta \\ &= \sum_{\gamma=0}^{\mathrm{No}}\omega_\gamma \nabla_U F(U^{\mathrm{P}}(\xi_\gamma);\xi_\gamma)\Psi_\alpha(\xi_\gamma)\left(\sum_{\beta=0}^{\mathrm{No}}\left(v_\eta^k\right)_\beta \Psi_\beta(\xi_\gamma)\right) \\ &= \sum_{\gamma=0}^{\mathrm{No}}\omega_\gamma \nabla_U F(U^{\mathrm{P}}(\xi_\gamma);\xi_\gamma)\Psi_\alpha(\xi_\gamma)V_\eta^k(\xi_\gamma) \\ &= \omega_\eta \Psi_\alpha(\xi_\eta)\nabla_U F(U^{\mathrm{P}}(\xi_\eta);\xi_\eta)W^k(\xi_\eta) = \omega_\eta\Psi_\alpha(\xi_\eta)\Lambda^k(\xi_\eta)W^k(\xi_\eta) = \Lambda^k(\xi_\eta)\left(v_\eta^k\right)_\alpha. \quad (34)\end{aligned}$$

The proof is complete. □

Therefore, in the most general case, $\nabla_u f \approx \overline{\nabla_u f}$, the latter matrix being $\mathbb{R}$-diagonalizable. Consequently, we can expect that provided the stochastic discretization is sufficiently accurate, the spectrum of $\overline{\nabla_u f}$ is a good approximation of the spectrum of $\nabla_u f$. This fact will be used for the computation of upwind matrices in the following section.

Finally, we observe that the extension to $\mathrm{N} > 1$ is straightforward owing to the full tensorization (of Gauss points and polynomial basis). The extension to $\mathrm{Nr} \geq 1$ is also straightforward.

4. Numerical method

The Galerkin system (15) is discretized using a FV method [12, 32]. Consider for simplicity a uniform spatial step Δx and discrete times t^n with time step $\Delta^n t = t^{n+1} - t^n$ verifying a CFL condition specified below. The FV scheme takes the form

$$u_i^{n+1} = u_i^n - \frac{\Delta^n t}{\Delta x}\left(\varphi(u_i^n, u_{i+1}^n) - \varphi(u_{i-1}^n, u_i^n)\right), \quad (35)$$

where u_i^n is an approximation to the mean value in space of the solution u in the cell of center $i\Delta x$ with width Δx at the time t^n and $\varphi(\cdot,\cdot)$ is the numerical flux function. The numerical flux is chosen in the form

$$\varphi(u_i^n, u_{i+1}^n) = \frac{f(u_i^n) + f(u_{i+1}^n)}{2} + a\,\frac{u_i^n - u_{i+1}^n}{2}, \quad (36)$$

where $\frac{1}{2}(f(u_i^n) + f(u_{i+1}^n))$ is the centered part of the flux and $a \in \mathbb{R}^{m(\mathrm{P}+1),m(\mathrm{P}+1)}$ is a (nonnegative) upwind matrix whose construction will be discussed in section 4.3.

4.1. Roe matrix and Roe state

We assume that the original stochastic problem (4) possesses a Roe matrix $A^{\mathrm{Roe}}(U_L, U_R; \xi) \in \mathbb{R}^{m,m} \otimes L^2(\Xi, p_\xi)$ almost surely. Recall that $A^{\mathrm{Roe}}(U_L, U_R; \xi)$ verifies the following properties:

- $A^{\mathrm{Roe}}(U_L, U_R; \xi)$ is $\mathbb{R}$-diagonalizable, $\forall U_L, U_R \in \mathcal{A}_U \otimes L^2(\Xi, p_\xi)$.
- Consistency with the stochastic Jacobian matrix $\nabla_U F$,

$$A^{\mathrm{Roe}}(U, U; \xi) = \nabla_U F(U; \xi), \quad \forall U \in \mathcal{A}_U \otimes L^2(\Xi, p_\xi).$$

- Conservativity through shocks,

$$F(U_R; \xi) - F(U_L; \xi) = A^{\mathrm{Roe}}(U_L, U_R; \xi)(U_R - U_L), \quad \forall U_L, U_R \in \mathcal{A}_U \otimes L^2(\Xi, p_\xi).$$

Theorem 4. *Under the above hypotheses, $\forall u_L, u_R \in \mathcal{A}_u$, the matrix $a(u_L, u_R) \in \mathbb{R}^{m(\mathrm{P}+1),m(\mathrm{P}+1)}$ defined by*

$$a(u_L, u_R) = \left\langle A^{\mathrm{Roe}}(U_L^{\mathrm{P}}, U_R^{\mathrm{P}}; \cdot)\Psi_\alpha \Psi_\beta \right\rangle_{\alpha,\beta=0,\ldots,\mathrm{P}} \tag{37}$$

with $U_L^{\mathrm{P}}(\xi) = \sum_{\alpha=0}^{\mathrm{P}} (u_L)_\alpha \Psi_\alpha(\xi)$ and $U_R^{\mathrm{P}}(\xi) = \sum_{\alpha=0}^{\mathrm{P}} (u_R)_\alpha \Psi_\alpha(\xi)$, verifies the following properties:

- *Consistency with the Galerkin Jacobian matrix $\nabla_u f$,*

$$a(u, u) = \nabla_u f(u), \quad \forall u \in \mathcal{A}_u.$$

- *Conservativity through shocks,*

$$f(u_R) - f(u_L) = a(u_L, u_R)(u_R - u_L), \quad \forall u_L, u_R \in \mathcal{A}_u.$$

Proof. To prove the consistency with the Galerkin Jacobian matrix, observe that $\forall u \in \mathcal{A}_u$, letting $U^{\mathrm{P}} = \sum_{\alpha=0}^{\mathrm{P}} u_\alpha \Psi_\alpha(\xi)$,

$$a(u, u) = \left(\left\langle A^{\mathrm{Roe}}(U^{\mathrm{P}}, U^{\mathrm{P}}; \cdot)\Psi_\alpha \Psi_\beta \right\rangle\right)_{\alpha,\beta=0,\ldots,\mathrm{P}} = \left(\left\langle \nabla_U F(U^{\mathrm{P}}; \cdot)\Psi_\alpha \Psi_\beta \right\rangle\right)_{\alpha,\beta=0,\ldots,\mathrm{P}} = \nabla_u f(u).$$

To prove the conservativity through shocks, observe that $\forall u_L, u_R \in \mathcal{A}_u$ and $\forall \alpha = 0, \ldots, \mathrm{P}$, letting $U_L^{\mathrm{P}} = \sum_{\alpha=0}^{\mathrm{P}} (u_L)_\alpha \Psi_\alpha(\xi)$ and $U_R^{\mathrm{P}} = \sum_{\alpha=0}^{\mathrm{P}} (u_R)_\alpha \Psi_\alpha(\xi)$,

$$\begin{aligned}
\left(f(u_R) - f(u_L)\right)_\alpha &= \left\langle \left(F(U_R^{\mathrm{P}}; \cdot) - F(U_L^{\mathrm{P}}; \cdot)\right) \Psi_\alpha \right\rangle = \left\langle A^{\mathrm{Roe}}(U_L^{\mathrm{P}}, U_R^{\mathrm{P}}; \cdot)(U_R^{\mathrm{P}} - U_L^{\mathrm{P}})\Psi_\alpha \right\rangle \\
&= \left\langle A^{\mathrm{Roe}}(U_L^{\mathrm{P}}, U_R^{\mathrm{P}}; \cdot) \sum_{\beta=0}^{\mathrm{P}} \left(\left\langle \Psi_\beta U_R^{\mathrm{P}} \right\rangle - \left\langle \Psi_\beta U_L^{\mathrm{P}} \right\rangle\right) \Psi_\alpha \Psi_\beta \right\rangle \\
&= \sum_{\beta=0}^{\mathrm{P}} \left\langle A^{\mathrm{Roe}}(U_L^{\mathrm{P}}, U_R^{\mathrm{P}}; \cdot)\Psi_\alpha \Psi_\beta \right\rangle \left(\left\langle \Psi_\beta U_R^{\mathrm{P}} \right\rangle - \left\langle \Psi_\beta U_L^{\mathrm{P}} \right\rangle\right) \\
&= \sum_{\beta=0}^{\mathrm{P}} (a)_{\alpha,\beta} \left((u_R)_\beta - (u_L)_\beta\right).
\end{aligned}$$

This completes the proof. □

Assume furthermore that for all $U_L, U_R \in \mathcal{A}_U \otimes L^2(\Xi, p_\xi)$, there exists a Roe state $U_{LR}^{\mathrm{Roe}} \in \mathcal{A}_U \otimes L^2(\Xi, p_\xi)$ almost surely such that

$$A^{\mathrm{Roe}}(U_L, U_R; \xi) = \nabla_U F(U_{LR}^{\mathrm{Roe}}; \xi), \tag{38}$$

and for all $(U_L^{\mathrm{P}}, U_R^{\mathrm{P}}) \in (\mathcal{A}_U \otimes L^2(\Xi, p_\xi))^2$, introduce the shorthand notation $U_{LR}^{\mathrm{Roe,P}} \in \mathcal{A}_U \otimes L^2(\Xi, p_\xi)$ such that $A^{\mathrm{Roe}}(U_L^{\mathrm{P}}, U_R^{\mathrm{P}}; \xi) = \nabla_U F(U_{LR}^{\mathrm{Roe,P}}; \xi)$. Then,

$$a(u_L, u_R) = \left\langle \nabla_U F(U_{LR}^{\mathrm{Roe,P}}; \cdot)\Psi_\alpha \Psi_\beta \right\rangle_{\alpha,\beta=0,\ldots,\mathrm{P}} = \nabla_u f(u_{LR}^{\mathrm{Roe}}), \tag{39}$$

with $u_{LR}^{\mathrm{Roe}} = (< \Psi_\alpha U_{LR}^{\mathrm{Roe,P}} >)_{\alpha=0,\ldots,\mathrm{P}}$, that is, a Roe state can also be defined for the Galerkin system. Moreover, if the Galerkin Jacobian matrix $\nabla_u f(u)$ is $\mathbb{R}$-diagonalizable for all $u \in \mathcal{A}_u$, then $\nabla_u f(u_{LR}^{\mathrm{Roe}})$ is a Roe linearized matrix.

4.2. An efficient method for approximating the absolute value of a matrix.

Let A be a deterministic $\mathbb{R}$-diagonalizable matrix of size N_A. By definition, $|A|$ is the co-diagonalizable matrix with A whose eigenvalues are the absolute values of those of A,

$$|A| = \sum_{i=1}^{\mathrm{N}_A} |\lambda_i| l_i \otimes r_i, \tag{40}$$

where $\{\lambda_i\}_{i=1,\dots,\mathrm{N}_A}$ are the real eigenvalues of A, $\{l_i\}_{i=1,\dots,\mathrm{N}_A}$ the left eigenvectors, and $\{r_i\}_{i=1,\dots,\mathrm{N}_A}$ the right eigenvectors. It is possible to diagonalize A and to compute $|A|$ using (40), but in practice this method is extremely costly. A more interesting method has been proposed in [28], which consists in computing a sequence of polynomial iterations based on the exact knowledge of the eigenvalues (or at last an explicit bound), and converging to the matrix sign if all the eigenvalues are real. However, this method also becomes costly when N_A grows. Another method has been proposed in [7], relying on the computation of a polynomial which interpolates some absolute values of the eigenvalues of A. We derive here a new method based on a single computation of a low-degree polynomial. Our method is clearly less costly, and it is also better adapted to the situations where only approximations of the eigenvalues are known. Denote by $\{\lambda'_i\}_{i=1,\dots,\mathrm{N}_A}$ the approximate eigenvalues of A. The method consists in finding a polynomial $q_{[d,\lambda'_i]}$ with degree d (d is fixed a priori) which minimizes the least-squares error between $|\lambda'_i|$ and $q(\lambda'_i)$, and then applying this polynomial to the matrix A in order to approximate $|A|$.

Let $q(X) = \sum_{j=0}^{d} c_j X^j$ be a polynomial. We seek $q_{[d,\lambda'_i]}$ which minimizes the error $\sum_{i=1}^{\mathrm{N}_A} \left(|\lambda'_i| - q_{[d,\lambda'_i]}(\lambda'_i)\right)^2$. It is well-known that this minimization problem is equivalent to solving a linear system with the polynomial coefficients $(c_j)_{j=0,\cdots,d}$ as unknows. This system of size $(d+1)\times(d+1)$ can be written as

$$\begin{pmatrix} \sum_{i=1}^{\mathrm{N}_A} {\lambda'}_i^0 \lambda'^0_i & \dots & \sum_{i=1}^{\mathrm{N}_A} {\lambda'}_i^0 \lambda'^d_i \\ \vdots & \ddots & \vdots \\ \sum_{i=1}^{\mathrm{N}_A} {\lambda'}_i^d \lambda'^0_i & \dots & \sum_{i=1}^{\mathrm{N}_A} {\lambda'}_i^d \lambda'^d_i \end{pmatrix} \begin{pmatrix} c_0 \\ \vdots \\ c_d \end{pmatrix} = \begin{pmatrix} \sum_{i=1}^{\mathrm{N}_A} |\lambda'_i| \lambda'^0_i \\ \vdots \\ \sum_{i=1}^{\mathrm{N}_A} |\lambda'_i| \lambda'^d_i \end{pmatrix}. \tag{41}$$

Solving this linear system yields the coefficients $(c_j)_{j=0,\cdots,d}$ that define the polynomial $q_{[d,\lambda'_i]}$. We then apply this polynomial to A and obtain an approximation to $|A|$. For efficiency, Hörner's method can be used: $q_{[d,\lambda'_i]}(A)$ can be rewritten as

$$q_{[d,\lambda'_i]}(A) = c_0 I + (c_1 I + (c_2 I + \cdots + (c_{d-1} I + c_d A)\dots A)A). \tag{42}$$

The number of matrix-matrix products is thus reduced to d and the computational cost is proportional to the polynomial degree d. We can further reduce the computational cost in cases where only the product of $|A|$ times a given vector x is needed. By computing directly $|A|x$, the cost is reduced to d matrix-vector products.

4.3. The upwind scheme

We apply the method presented in the previous section to approximate the absolute value of $\nabla_u f(u_{LR}^{\mathrm{Roe}}) \in \mathbb{R}^{m(\mathrm{P}+1),m(\mathrm{P}+1)}$ at each interface LR in physical space. To this purpose, we use as approximate eigenvalues $\{\lambda'_i\}_{i=1,\dots,m(\mathrm{P}+1)}$, the eigenvalues of the stochastic Jacobian matrix $\nabla_U F$ evaluated at $U_{LR}^{\mathrm{Roe,P}}(\xi) = \sum_{\alpha=0}^{\mathrm{P}} (u_{LR}^{\mathrm{Roe}})_\alpha \Psi_\alpha(\xi)$ and at the Gauss points of each stochastic element. Choosing a degree d then yields a polynomial $q_{[d,\lambda'_i]}$. An important remark is that the linear system (41) can be singular if the number of disctinct eigenvalues λ'_i is less than d. In particular, this occurs in the deterministic case. To properly handle this issue, we use a Singular Value Decomposition method.

We choose to work with the SE basis. In particular, we recall that with this basis, the Galerkin Jacobian matrix $\nabla_u f$ has a diagonal block structure. Therefore, the above procedure can be applied separately to each stochastic element. The key advantage is that the polynomial is different for each stochastic element and has to fit less points than in the case of the global MW basis. Thus, computations are at the same time more efficient and more accurate.

The numerical flux in the Finite Volume scheme (35) is chosen in the form

$$\varphi(u_i^n, u_{i+1}^n) = \frac{f(u_i^n) + f(u_{i+1}^n)}{2} + q_{[d,\lambda'_i]}(\nabla_u f(u_{i,i+1}^{\mathrm{Roe}}))\ \frac{u_i^n - u_{i+1}^n}{2}. \tag{43}$$

We emphasize that this numerical flux is not a projection of the flux of the original stochastic problem (4) as some methods discussed in the introduction propose, but a numerical flux associated with the Galerkin system (15).

Finally, the time-step $\Delta^n t$ is selected from a CFL-condition based on the highest characteristic velocity over the spatial and stochastic discretization cells. In practice, $\Delta^n t$ is computed such that

$$\frac{\Delta^n t}{\Delta x} = \frac{C}{\max\limits_{LR\in\mathcal{I},i=1,\dots,m(\mathrm{P}+1)} |\lambda_i'(u_{LR}^{\mathrm{Roe}})|}, \tag{44}$$

where $\mathcal{I}$ denotes the set of interfaces LR and $(\lambda_i')_{i=1,\dots,m(\mathrm{P}+1)}$ are the approximate eigenvalues identified above. In the sequel, we set the CFL constant C to 0.95.

We observe that the matrix $q_{[d,\lambda_i']}(\nabla_u f(u_{i,i+1}^{\mathrm{Roe}}))$ is not guaranteed to control the eigenvalues of $\nabla_u f(u_{i,i+1}^{\mathrm{Roe}})$ and it is not even guaranteed to be nonnegative. Indeed, approximate eigenvalues of $\nabla_u f(u_{i,i+1}^{\mathrm{Roe}})$ have been used to build $q_{[d,\lambda_i']}$, and, in addition, this polynomial only provides a least-square fit to the eigenvalues. This issue can possibly be handled by lowering the CFL constant C.

5. Results

The methodology presented in the previous sections is assessed on three test cases. The first two deal with the Burgers equation and the third one with the Euler equations.

5.1. Test case 1: Burgers equation

The goal of this first test case is to assess the proposed methodology for a stochastic scalar conservation law (the Burgers equation) so that the Galerkin system is guaranteed to be hyperbolic from theorems 1 or 2, and involving only a positive wave speed so that the computation of $|\nabla_u f(u_{LR}^{\mathrm{Roe}})|$ is trivial.

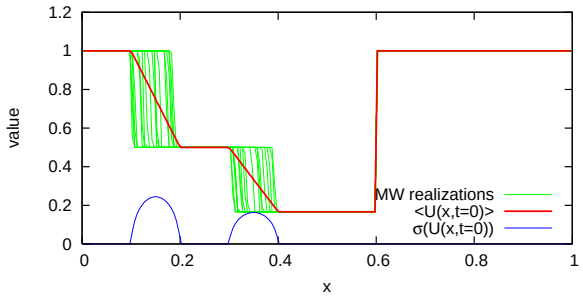

Figure 1: Random initial condition for test case 1: sample set of 20 random realizations, mean, and standard deviation.

5.1.1. Problem definition

We consider a one-dimensional spatial domain $\Omega = [0, 1]$ with periodic boundary conditions. The governing equation, in conservative form, is

$$\frac{\partial U}{\partial t} + \frac{\partial F(U)}{\partial x} = 0, \quad F(U) = \frac{U^2}{2}, \tag{45}$$

and we consider an uncertain initial condition $U^0(x, \xi)$ consisting of three piecewise constant deterministic states in x. Specifically, the three states are $\overline{u}^1 = 1$, $\overline{u}^2 = 1/2$, and $\overline{u}^3 = 1/6$, and the position of some jumps is uncertain: the jump from states $\overline{u}^1$ to $\overline{u}^2$ occurs at a random location $X_{1,2}$ having a uniform distribution in $[0.1, 0.2]$, while the jump from states $\overline{u}^2$ to $\overline{u}^3$ occurs at a random location $X_{2,3}$ having a uniform distribution in $[0.3, 0.4]$. Finally, the jump from states $\overline{u}^3$ to $\overline{u}^1$ is at $x_{31} = 0.6$. The random locations $X_{1,2}$ and $X_{2,3}$ are independent and parameterized using two independent random variables ξ_1 and ξ_2 respectively, both with uniform distribution in $[0, 1]$:

$$X_{1,2} = 0.1 + 0.1\xi_1, \quad X_{2,3} = 0.3 + 0.1\xi_2, \quad \xi_1, \xi_2 \sim \mathcal{U}[0, 1]. \tag{46}$$

Therefore, the problem has two stochastic dimensions (N = 2), and the dimension of the approximation space for expansion order No and resolution level Nr is

$$\dim \mathcal{S}^{\mathrm{No,Nr}} = (\mathrm{No}+1)^2 2^{2\mathrm{Nr}}. \tag{47}$$

The initial condition is discretized on the mesh by taking cell averaged random states as initial values. At the stochastic level, the discretization uses piecewise continuous bilinear approximations over the $2^{2\mathrm{Nr}}$ stochastic elements for No ≥ 1, or the stochastic element averaged state for No $= 0$. The bilinear approximation is constructed such that initial discrete states are continuous in the stochastic domain. This procedure prevents the presence of overshoots in the initial data. However, no particular treatment is applied to enforce the stochastic continuity during time integration. In Figure 1, we provide an illustration of the random initial condition for a spatial discretization with Nc = 200 uniform cells in physical space. The plot shows a sample set of 20 realizations of the random initial condition $U^0(x,\xi)$, with its expectation and standard deviation. It can be observed that the realizations present slightly inclined shocks, an effect caused by the cell average procedure and which can be reduced by taking a finer spatial mesh.

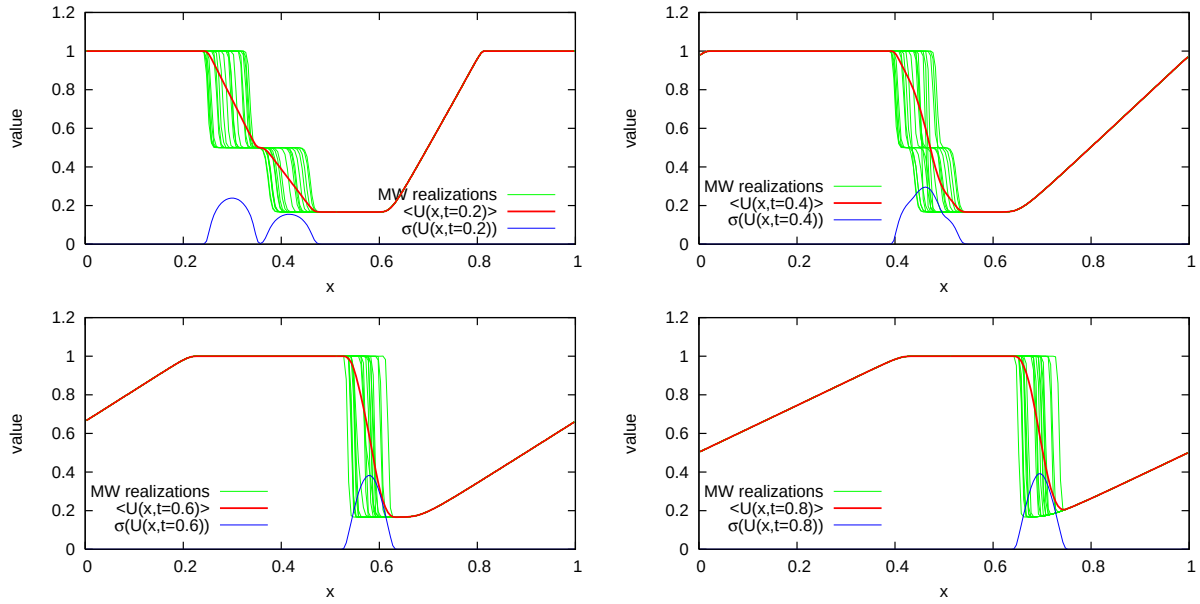

Figure 2: Solution of the stochastic Burgers equation at $t = 0.2$, 0.4, 0.6, and 0.8. The solution mean (red) and standard deviation (blue) are plotted as a function of x, together with a reconstruction of 20 randomly generated realizations (green). Computations with Nr = 3 and No = 3.

5.1.2. Time integration

The stochastic Burgers equation is time-integrated using the Roe solver described above. We recall that since U is a scalar, the Galerkin problem is hyperbolic. The stochastic discretization is performed using the SE basis. Moreover, the evaluation of the stochastic expansion of the nonlinear flux $F(U)$ relies on pseudo-spectral methods that will be detailed in section 5.3.

It is well-known that for the deterministic Burgers equation, the eigenvalue of the stochastic Jacobian matrix $\nabla_U F$ is U. Because in the present setting the initial condition is almost surely positive for any x, we expect $U > 0$ with probability one, for all (x,t). Therefore, the spectrum of the Galerkin Jacobian matrix is expected to be strictly positive, so that the upwinding matrix of the Galerkin problem reduces to the Galerkin Jacobian matrix (the polynomial transformation is in fact the identity).

In Figure 2 we show the stochastic solution at times $t = 0.2$, 0.4, 0.6, and 0.8. The computation uses Nr = 3 and No = 3, so that the dimension of the stochastic space is $16 \times 64 = 1024$. The solution expectation

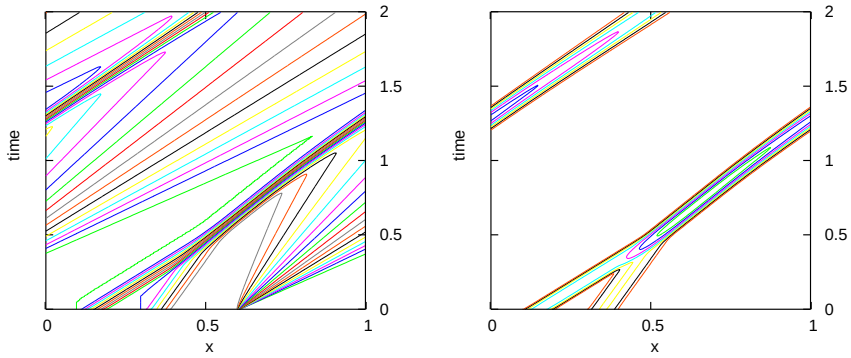

Figure 3: Space-time diagrams of the expectation (left) and standard deviation (right) of the stochastic Burgers solution. Contours are in the range $[0, 1]$ with a constant spacing 0.05. Computations with Nr = 3 and No = 3.

and standard deviation, together with a random sample set of realizations are also plotted. The realizations are reconstructed from the stochastic expansions of the solutions, using a unique set of randomly generated realizations of $\xi \in [0, 1]^2$.

Focusing first on the stochastic solution, we observe that the proposed method correctly captures the dynamics of the Burgers equation. The shocks are transported with the correct velocity and the discontinuities remain sharp as time evolves. For $t = 0.2$, the first shock whose velocity is 0.75 has not yet reached the second shock whose velocity is $1/3$. At $t = 0.4$, a fraction of the realizations corresponds to a situation where the first and second shocks have merged. At $t = 0.6$, the shocks have merged for nearly all realizations, a situation which is fully achieved at $t = 0.8$. It can be observed that the realizations, although corresponding to the same sample set of ξ in all plots, present a different distribution before and after the shocks have merged. Indeed, since the merging happens at different times depending on the initial locations of the two shocks and the shock velocities are different before and after merging, the final location of the shock is not expected to be uniform.

The uncertain shock dynamics can also be analyzed from the standard deviations of the stochastic solution: not only the maximum standard deviation is larger at $t = 0.8$, denoting the higher amplitude of the discontinuity, but the profiles are different. The expectation plots confirm the previous observations. While the uncertainty in shock location induces an affine evolution of $\langle U \rangle$ when the two shocks are distinct, a variable slope of $\langle U \rangle$ with x is observed after the shocks have merged: this indicates a non-uniform distribution of the final shock location. Similarly, the dynamics of the (deterministic) rarefaction wave is well captured.

In addition to the analysis of the uncertain shocks dynamics, Figure 2 also demonstrates that the Roe solver for the Galerkin system does not create spurious uncertainty in the solution, through numerical diffusion for instance. This can be better seen from Figure 3 where the space-time diagrams of the solution expectation and standard deviation are plotted over the larger period of time $t \in [0, 2]$. For time $t > 0.7$, in a moving frame attached to the remaining shock, the standard deviation reaches a maximum at $t \approx 1$ where it peaks at $\sigma(U) \approx 0.42$, and then slowly decays. This decay is not a numerical artifact, but is induced by the rarefaction wave which has grown up to occupy the whole domain, as seen from the expectation plot where the plateau $U = 1$ has disappeared for $t > 1$.

For analysis purpose, we define a moving observation point $x_o(t) = 0.25 + 0.5t$. The observation point is initially located between the two stochastic shocks. Since the velocity of x_o is lower than 0.75, x_o will be caught-up by the first random shock. Moreover, since x_o moves faster than the second shock, there is a time interval for which the stochastic solution at x_o corresponds to a set of events ξ with different configurations of the shocks. This is seen from Figure 4 where the stochastic solution $U(x_o(t), t, \xi)$ is plotted as a function of $\xi = (\xi_1, \xi_2)$ for various times $t \in [0.2, 0.7]$. For $t = 0.2$, the observation point starts to be caught-up by some events corresponding to the largest realizations of $X_{1,2}$: the solution is a function of ξ_1 only. At $t = 0.3$, a larger fraction (roughly $1/4$) of the first shock has overrun the observation point, and the stochastic solution

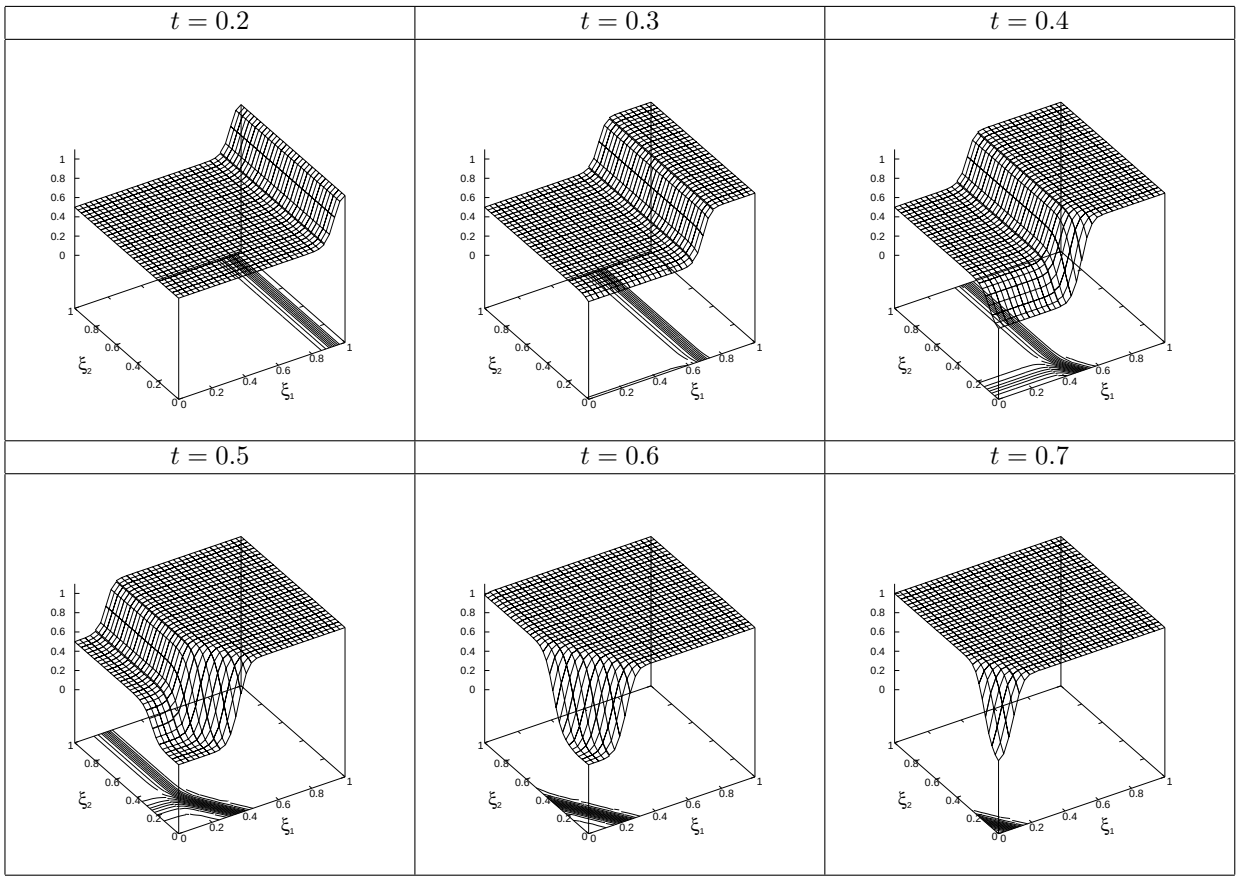

Figure 4: Stochastic solution of the Burgers equation at observation point $x_o(t)$ as a function of (ξ_1, ξ_2) and for different times as indicated. Computations with No = 3 and Nr = 3.

exhibits two plateaus. At $t = 0.4$, the observation point starts to reach the second shock, introducing some dependence on ξ_2, while a fraction of events corresponds to shocks having merged. This creates a stochastic solution with three distinct plateaus with respective values 1, 1/2, and 1/6, whose configuration evolves in time. At $t = 0.7$, the solution at the observation point is essentially constant and equal to 1, with only a small fraction of events for which $U = 1/6$.

These results demonstrate the ability of the proposed method to account for nonlinear dynamics and complex interaction between random shocks. However, plots in Figure 4 deserve more comments. Firstly, although the multi-resolution scheme allows for discontinuities across the stochastic discretization cells, the solutions reported here appear essentially continuous. While the initialization procedure ensures stochastic continuity of the initial condition, the numerical method maintains satisfactorily this property as time advances, as expected from the properties of the Burgers equation, provided that the resolution is fine enough. Secondly, the transitions between the states are smooth. This is due to the numerical diffusion of the Roe method which is known to spread the shocks on a few spatial cells. The smoothness of the stochastic solution reflects this spatial numerical diffusion. This point will be further evidenced below, where we show that the smooth transitions in the stochastic domain have a characteristic thickness independent of the stochastic resolution. In addition, we can observe that the smooth transitions are thicker along the second (ξ_2) stochastic direction than along the first (ξ_1). This is due to the different shock velocities (effects of different local CFLs).

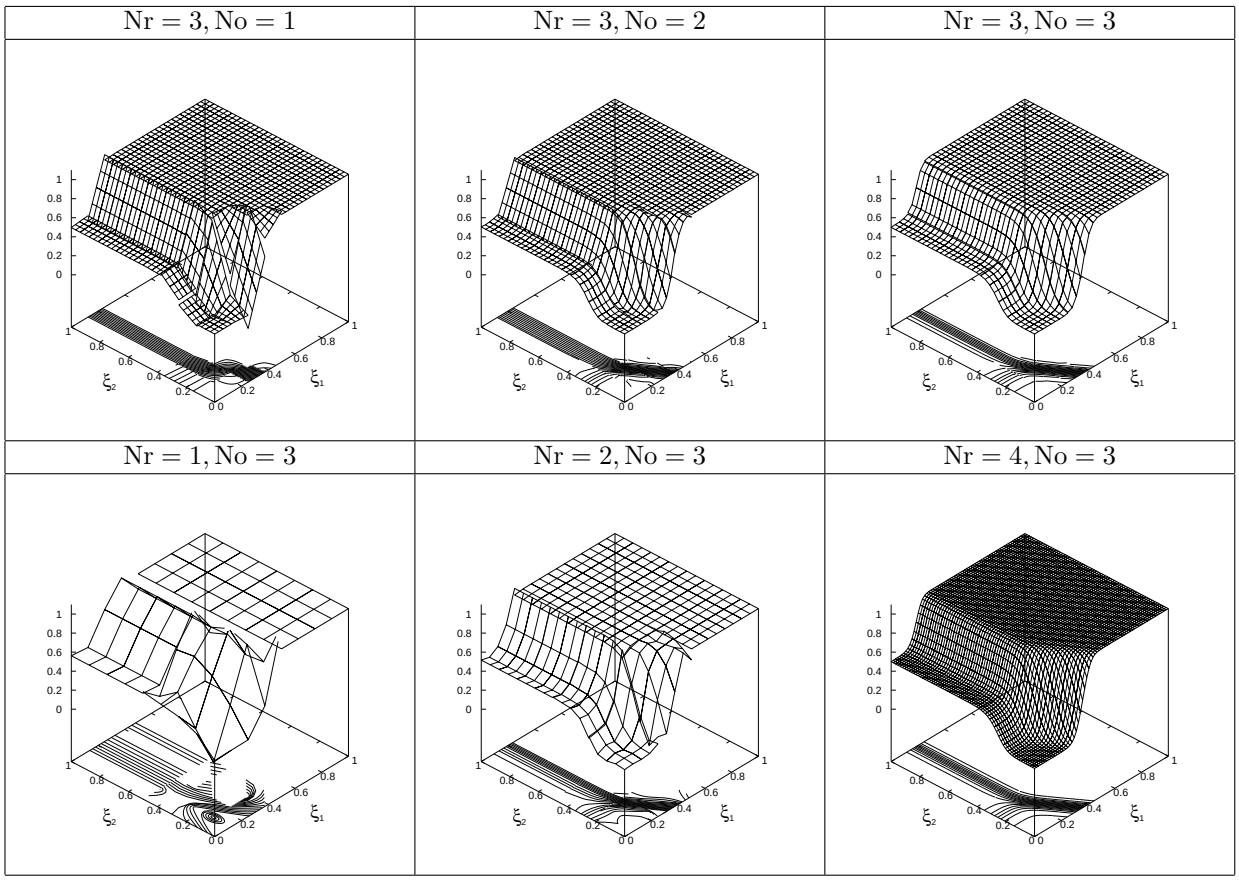

Figure 5: Stochastic solutions of the Burgers equation as a function of (ξ_1, ξ_2) at $x = 0.5$ and time $t = 0.5$ for different stochastic discretization parameters Nr and No as indicated.

5.1.3. Convergence analysis

We present in Figure 5 the stochastic solutions at the observation point x_o and $t = 0.5$ for different stochastic discretizations. The plots of the first line illustrate the convergence of the approximation with the expansion order No, while those of the second line highlight the convergence with the resolution level Nr. It is seen that when the stochastic discretization is too coarse, the solution exhibits significant discontinuities between stochastic discretization cells. Moreover, as claimed above, the transition thicknesses in the stochastic domain becomes independent of No and Nr as they increase.

5.2. Test case 2: Burgers equation

The purpose of this test case is to assess the method still for the Burgers equation (so that the Galerkin system is guaranteed to be hyperbolic), but in a situation involving positive and negative wave speeds thereby requiring the calculation of $|\nabla_u f(u_{LR}^{\text{Roe}})|$ as outlined in sections 4.2 and4.3.

5.2.1. Problem definition

We still consider the Burgers equation, but with stochastic initial condition $U^0(x, \xi)$ defined using two uncertain states, $U^+(\xi_1)$ and $U^-(\xi_2)$, the first one almost surely positive and the second one almost surely

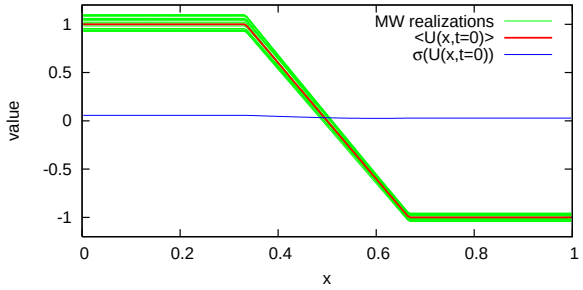

Figure 6: Random initial condition for test case 2: sample set of 20 random realizations, mean, and standard deviation.

negative. We take for $x \in [0,1]$,

$$U^0(x,\xi) = \begin{cases} U^+(\xi_1) & x < 1/3, \\ U^-(\xi_2) & x > 2/3, \\ U^+(\xi_1)(2-3x) + U^-(\xi_2)(3x-1) & 1/3 \le x \le 2/3, \end{cases} \tag{48}$$

such that $U^0(x,\xi)$ is continuous for any $\xi \in [0,1]^2$. We define the stochastic states as

$$\begin{aligned} U^+(\xi_1) &= 1 + 0.1(2\xi_1 - 1), \qquad & \xi_1 \sim \mathcal{U}[0,1] \to U^+ \sim \mathcal{U}[0.9, 1.1], \\ U^-(\xi_2) &= -1 + 0.05(2\xi_2 - 1), \qquad & \xi_2 \sim \mathcal{U}[0,1] \to U^- \sim \mathcal{U}[-1.05, -0.95], \end{aligned} \tag{49}$$

and we solve the stochastic Burgers equation with Dirichlet boundary conditions, $U = U^+$ at $x = 0$ and $U = U^-$ at $x = 1$. The initial condition is illustrated in Figure 6. Nc $= 200$ cells are used for space discretization.

5.2.2. Time integration

Although initially continuous, the stochastic solution will develop in finite time a discontinuity with a stochastic jump $|U^+ - U^-|$ and a stochastic propagation velocity $(U^+ + U^-)/2$. The stochastic character of the shock magnitude and velocity has to be contrasted with the situation of the previous test case, where the jumps and shock velocity were certain. This yields a much more complex situation as illustrated in Figure 7 where the solution is plotted at different times for the stochastic discretization parameters No $= 3$ and Nr $= 3$ so that $\dim \mathcal{S}^{\mathrm{No,Nr}} = 1024$.

From the realizations plotted in Figure 7, we can observe the appearance of overshoots which are a direct consequence of the shock formation and its uncertain propagation velocity. To get further insight, we present in Figure 8 the evolution of the solution at a fixed point $x_o = 0.5$ and different times. The plots show the evolution from the initially smooth solution to a shocked solution with states U^+ or U^- according to the sign of $2(\xi_1 - 1/2) - (\xi_2 - 1/2)$. In addition, it is seen that overshoots occur only in a neighborhood of the discontinuity, namely in stochastic elements containing the developping discontinuity. Using a finer stochastic discretization (increasing Nr) delays the emergence of the overshoots and reduces the portion of the stochastic domain affected by them.

5.2.3. Validation of the method used to evaluate the upwinding matrix

Another interesting property of the present test case is that contrary to the previous one, there exist spatial cells where the solution U can take positive and negative values. As a result, the eigenvalues of the Galerkin Jacobian matrix $\nabla_u f$ are no longer always positive, and the polynomial transformation q to approach the absolute value of $\nabla_u f(u_{LR}^{\mathrm{Roe}})$ is no longer trivial as in the previous example. We then investigate the impact of the selected polynomial degree d of q on the computed solution. In the example presented previously, we used polynomials with degree $d = 3$. In Figure 9 we report the stochastic solution at $x = 0.5$ and $t = 0.5$ as computed using increasing polynomial degree d. It is seen that for $d = 1$, the solution

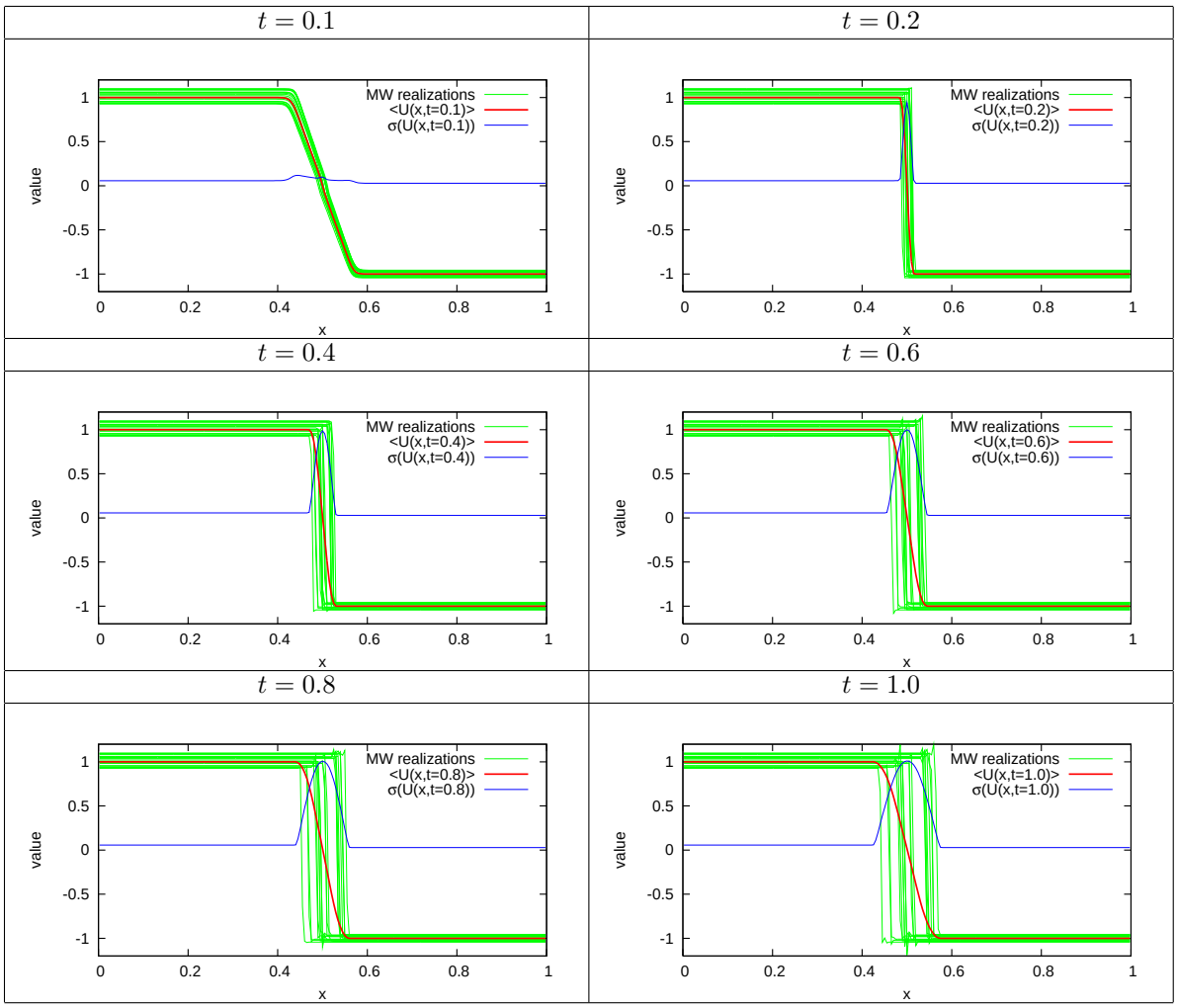

Figure 7: Stochastic solution of the Burgers equation at different times. The solution mean (red) and standard deviation (blue) are plotted as a function of x, together with a reconstruction of 20 randomly generated realizations of the solution (green). Computations with Nr = 3 and No = 3.

exhibits significant discontinuities and overshoots across the stochastic discretization cells containing the developping shock (where the solution changes sign). When $d = 2$, the overshoots and discontinuities are greatly reduced compared to the case $d = 1$. Increasing further d does not bring significant improvement in the solution. In fact, at that stage the error in the solution isessentially dominated by the stochastic and spatial discretization error, whereby the error in the approximation of $|\nabla_u f(u_{LR}^{\text{Roe}})|$ for $d > 3$ is negligible.

To measure more precisely the error on the approximation of $|\nabla_u f(u_{LR}^{\text{Roe}})|$, we compute the set of exact eigenvalues $\{\lambda_\alpha\}_{\alpha=0,\dots,\text{P}}$ of the Galerkin Jacobian matrix $\nabla_u f$. We then compare the quantities $|\lambda_\alpha|$ with their respective polynomial approximation $q(\lambda_\alpha)$. The error is quantified using the L_2 and L_∞ measures, defined respectively as

$$\epsilon_2^2 = \frac{1}{\text{P}} \sum_{\alpha=0}^{\text{P}} \left(|\lambda_\alpha| - q(\lambda_\alpha)\right)^2, \qquad \epsilon_\infty = \max_{0 \le \alpha \le \text{P}} ||\lambda_\alpha| - q(\lambda_\alpha)|. \tag{50}$$

In Figure 10 we present the error measures at $t = 0.4$ as a function of x. We first remark that the error is limited to the portion of the spatial domain where the stochastic shock can be present, and diminishes as d increases. The error measures appear to stagnate when d increases beyond 5 as one may have expected

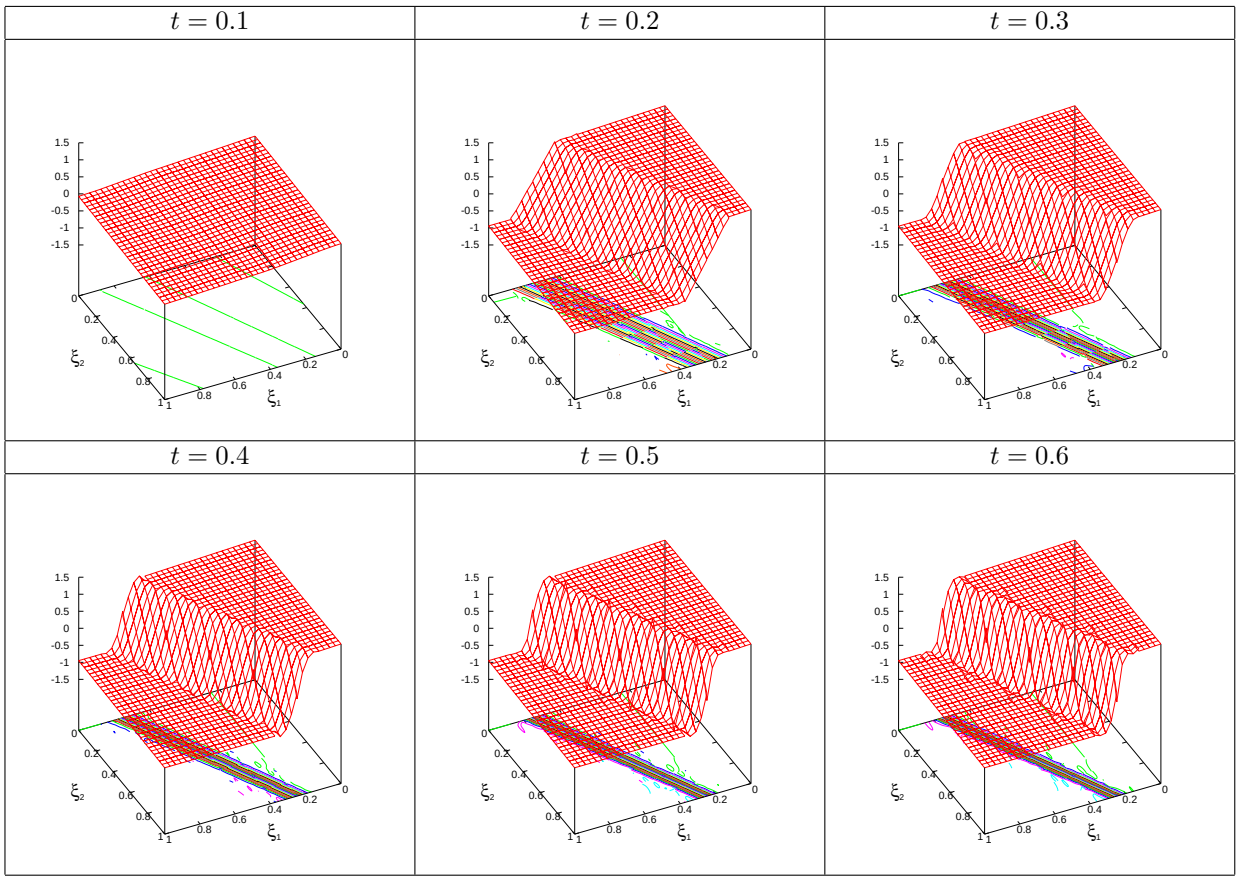

Figure 8: Stochastic solution of the Burgers equation as a function of (ξ_1, ξ_2) at $x = 0.5$ and different times as indicated. Computations with Nr = 3 and No = 3.

since the computations here use No = 3, so that the estimated eigenvalues (at the tensorized Gauss points) used for the determination of q are not the actual eigenvalues of $\nabla_u f$.

5.2.4. Convergence of the stochastic error

We take advantage of this simple problem setting to investigate the convergence of the stochastic solution. Indeed, for this Riemann problem, we can easily derive the exact solution $U(x, t, \xi)$ for any given ξ, hereafter denoted U_{ex}, as long as the shock has not reached one of the domain boundaries [12]. We rely on a Monte-Carlo sampling strategy to estimate the two first moments of U_{ex}. We proceed as follows. Firstly, a random sample set of M realizations of ξ is generated by sampling uniformly $[0, 1]^2$. Secondly, for each element $\xi^{(i)}$ of the sample set, we define $u^{(i)}(x, t) \equiv U_{ex}(x, t, \xi^{(i)})$ for $i = 1, \ldots, M$. The sample set estimate of the mean is

$$\langle U_{ex} \rangle (x, t) \approx \frac{1}{M} \sum_{i=1}^{M} u^{(i)}(x, t) = E_s(U_{ex})(x, t), \tag{51}$$

while the sample set estimate of the standard deviation of is

$$\sigma^2(U_{ex})(x, t) \approx \frac{1}{M} \sum_{i=1}^{M} \left(u^{(i)} - E_s(U_{ex}) \right)^2 (x, t) = \sigma_s^2(U_{ex})(x, t). \tag{52}$$

To minimize the random sampling error in the sample estimate, we use $M = 100000$.

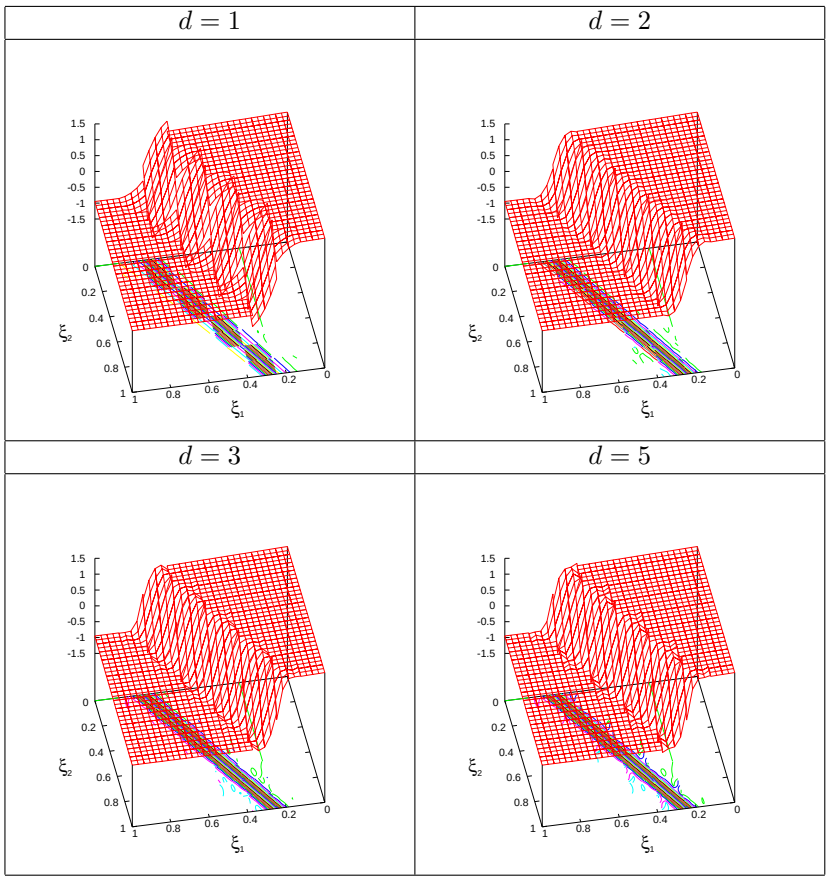

Figure 9: Stochastic solution of the Burgers equation as a function of (ξ_1, ξ_2) at $x = 0.5$ and $t = 0.5$ and for different degrees d of the polynomial q to approximate the absolute value of $\nabla_u f(u_{LR}^{\text{Roe}})$. Computations with $\text{Nr} = 3$ and $\text{No} = 3$.

In Figure 11, we compare the mean and standard deviation of the exact and computed solution for $\text{No} = 2$ and $\text{Nr} = 4$ at $t = 0.6$ on a mesh with $\text{Nc} = 201$ cells. It is seen that the means of the computed and exact solutions are in excellent agreement. For the standard deviations, computed and exact solutions are again in agreement, although one can notice that the computed solution slightly under-estimates the standard deviation with less than 5% of relative error. Using a finer stochastic discretization only marginally improves the error on the standard deviation, since the error in U is here dominated by the spatial discretization error. This is demonstrated in Figure 12, where the difference in the computed and exact standard deviations is plotted for finer and finer spatial meshes. One observes that for $\text{Nc} = 501$, the discretization error has reached the level of the stochastic discretization error.

To further analyze the stochastic convergence of the method, we monitor the convergence of the semi-discrete stochastic solution, discretized on a fixed spatial mesh. In the following, we set $\text{Nc} = 301$. We define the error measure on the semi-discrete solution as

$$\epsilon_h^2 \equiv \int_\Omega \left\langle \left(U_h^{\text{No,Nr}}(x,t,\cdot) - U_h^{ex}(x,t,\cdot) \right)^2 \right\rangle \mathrm{d}x, \tag{53}$$

where $U_h^{\text{No,Nr}}$ and U_h^{ex} are the computed and exact semi-discrete solutions. Since the latter is unknown, we again rely on a Monte Carlo estimation,

$$\epsilon_h^2 \approx \frac{1}{M} \sum_{i=1}^{M} \int_\Omega \left(U_h^{\text{No,Nr}}(x,t,\xi^{(i)}) - U_h^{ex}(x,t,\xi^{(i)}) \right)^2 \mathrm{d}x, \tag{54}$$

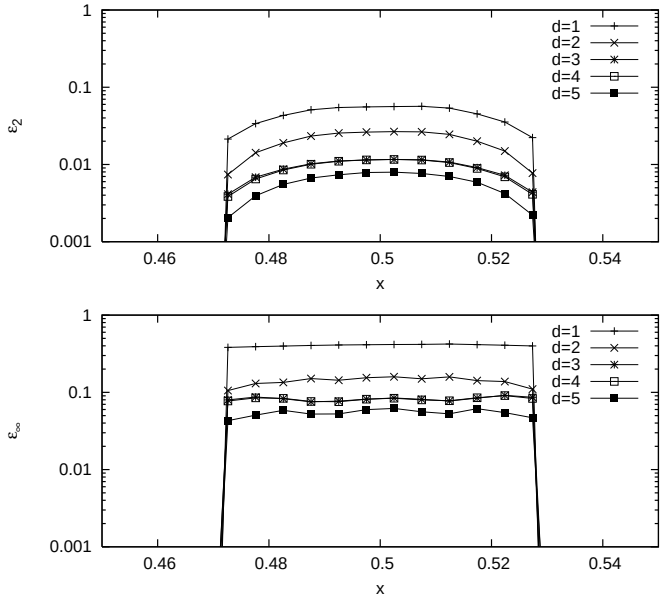

Figure 10: Measures ϵ_2 (top) and ϵ_∞ (bottom) of the errors on the eigenvalues of the absolute value of $\nabla_u f(u_{LR}^{\mathrm{Roe}})$ at time $t = 0.4$ and different degrees d of the polynomial q. Computations with $\mathrm{Nr} = 3$ and $\mathrm{No} = 3$.

where $U_h^{\mathrm{No,Nr}}(x, t, \xi^{(i)})$ and $U_h^{ex}(x, t, \xi^{(i)})$ are evaluated from the stochastic expansion of the computed solution and solving the corresponding deterministic (discrete) Burgers problem respectively, for each element $\xi^{(i)}$ in the sample set. We use a sample set dimension $M = 10000$. Figure 13 reports the stochastic error ϵ_h^2, at time $t = 0.6$, as a function of the resolution level Nr and for expansion orders $\mathrm{No} = 1, 2$ and 3. In this simulations, the approximation of the upwind matrix uses a polynomial degree defined as $d = min(8, \mathrm{P})$. We observe the decay of the stochastic error for both increasing resolution level and expansion order. For $\mathrm{Nr} = 0$ and $\mathrm{No} = 3$, the simulation is unstable due to the large error level.

5.3. Test case 3: Euler equations

In this section, the method is tested on the stochastic Euler equations with one random parameter. The goal of this test case is to assess the method on a non linear hyperbolicsystem of conservation laws, so that the obtained Galerkin system is not proven to be hyperbolic. We consider the one-dimensional Sod shock tube

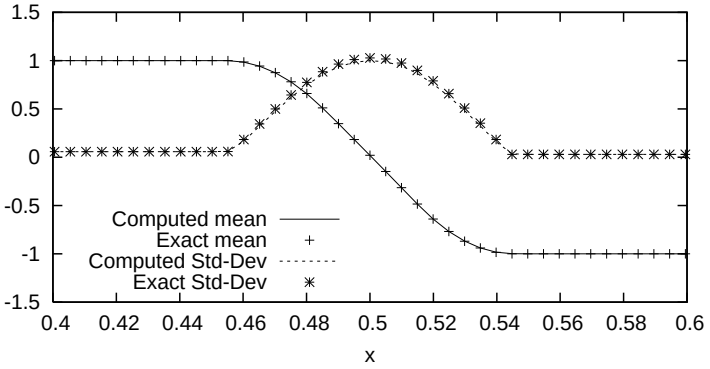

Figure 11: Comparison of the mean and standard deviation of the numerical solution at $t = 0.6$, computed with $\mathrm{No} = 2$, $\mathrm{Nr} = 4$ and $\mathrm{Nc} = 201$, with the corresponding MC estimates of the exact solution of the stochastic Burgers equation. Only a portion of the computational domain is shown for clarity.

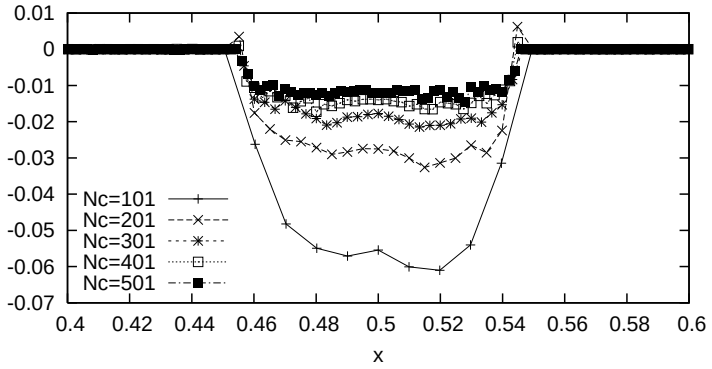

Figure 12: Differences in the computed and exact standard deviations at $t = 0.6$ for different spatial meshes. The numerical method uses No = 2 and Nr = 4. Only a portion of the computational domain is shown for clarity.

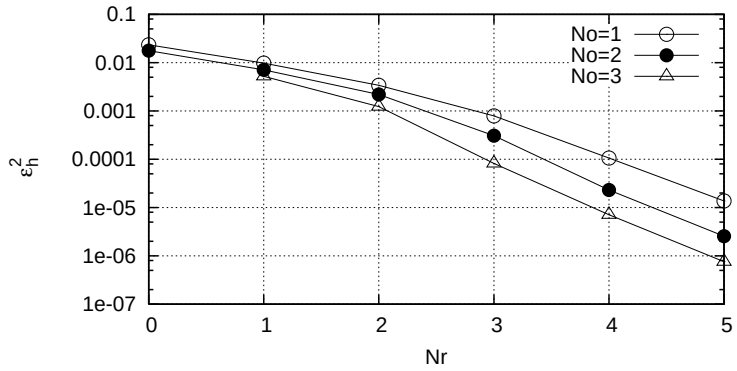

Figure 13: Stochastic error at $t = 0.6$ on the semi-discrete solution (see equation (53)) as a function of the resolution level Nr and for different expansion orders No as indicated. The semi-discrete solution is defined on a mesh with Nc = 301.

problem, where the flow of an ideal gas is governed by the Euler equations. Conventional thermodynamic notation is used instead of the lower/upper case convention adopted previously. The conserved quantities are the fluid density ρ, the impulse $q = \rho v$ (with v the velocity), and the total energy $E = 1/2\rho v^2 + \rho e$, where the first term is the kinetic energy and the second one the internal energy (per unit volume). The tube extends over one unit of length and is closed by two rigid walls at $x = 0$ and $x = 1$. Boundary conditions are $q = 0$ and $\frac{\partial \rho}{\partial x} = \frac{\partial E}{\partial x} = 0$ at the solid walls. The discretization makes use of Nc = 250 cells in physical space.

5.3.1. Problem definition

Recall that in the deterministic Euler equations, the conservative variables and fluxes are

$$\mathfrak{u} = (\rho, q, E), \quad \mathfrak{f}(\mathfrak{u}) = (\mathfrak{f}^\rho(\rho, q, E), \mathfrak{f}^q(\rho, q, E), \mathfrak{f}^E(\rho, q, E)) = (\rho v, \rho v^2 + p, v(E + p)), \tag{55}$$

with the velocity $v = q/\rho$ and the pressure p given by the ideal gas law

$$p = p(\rho, q, E) = (\gamma - 1)\left(E - \frac{1}{2}\rho v^2\right), \tag{56}$$

where $\gamma > 1$ is the adiabatic coefficient. The initial conditions are

$$\rho^0(x) = \begin{cases} 1 & x \in [0, 1/2], \\ 0.125 & x \in]1/2, 1], \end{cases} \quad v^0(x) = 0, \quad \text{and} \quad p^0(x) = \begin{cases} 1 & x \in [0, 1/2], \\ 0.125 & x \in]1/2, 1]. \end{cases} \tag{57}$$

We recall the deterministic Jacobian matrix

$$J(\mathfrak{u}) = \begin{pmatrix} 0 & 1 & 0 \\ 1/2(\gamma-3)v^2 & -(\gamma-3)v & \gamma-1 \\ 1/2(\gamma-1)v^3 - vH & H-(\gamma-1)v^2 & \gamma v \end{pmatrix}, \tag{58}$$

where $H = (E+p)/\rho$ is the enthalpy. The eigenvalues of $J(\mathfrak{u})$ are $v \pm c$ and v where c is the sound velocity such that $c^2 = (\gamma-1)(H - \frac{1}{2}\rho v^2)$. Moreover, with obvious notation, the Roe state is such that

$$\rho^{\text{Roe}} = \sqrt{\rho_L \rho_R}, \quad v^{\text{Roe}} = \frac{\sqrt{\rho_L}v_L + \sqrt{\rho_R}v_R}{\sqrt{\rho_L}+\sqrt{\rho_R}}, \quad H^{\text{Roe}} = \frac{\sqrt{\rho_L}H_L + \sqrt{\rho_R}H_R}{\sqrt{\rho_L}+\sqrt{\rho_R}}. \tag{59}$$

We consider an uncertainty on the adiabatic coefficient γ which is parametrized using a unique random variable ξ having a uniform distribution in $[0,1]$. We consider a uniform probability distribution of γ in the range $[1.4, 1.6]$, so that the parametrization is

$$\gamma(\xi) = 1.4 + 0.2\ \xi, \quad \xi \sim U[0,1]. \tag{60}$$

Consistently with the notation introduced above, we set

$$U(x,t,\xi) = (\rho(x,t,\xi), q(x,t,\xi), E(x,t,\xi)) \in \mathcal{A}_U \otimes L^2(\Xi, p_\xi), \tag{61}$$

and

$$F(U;\xi) = (F^\rho(U(x,t,\xi)), F^q(U(x,t,\xi);\xi), F^E(U(x,t,\xi);\xi)) \in \mathbb{R}^3 \otimes L^2(\Xi, p_\xi), \tag{62}$$

where $\mathcal{A}_U \subset \mathbb{R}^3$ is the set of admissible states such that the density and the pressure are positive.

5.3.2. Numerical solver

Computation of the Galerkin flux $f(u) \in \mathbb{R}^{3(\mathrm{P}+1)}$. For given expansions of $\rho(\xi) = \sum_{\alpha=0}^{\mathrm{P}} \rho_\alpha \Psi_\alpha(\xi)$, $q(\xi) = \sum_{\alpha=0}^{\mathrm{P}} q_\alpha \Psi_\alpha(\xi)$, and $E(\xi) = \sum_{\alpha=0}^{\mathrm{P}} E_\alpha \Psi_\alpha(\xi)$, we have to compute the stochastic modes $(f^\rho)_\alpha$, $(f^q)_\alpha$, and $(f^E)_\alpha$. The stochastic modes of $F^\rho(\cdot;\xi)$ are immediately obtained from

$$(f^\rho)_\alpha = \left\langle F^\rho(U^P;\cdot)\Psi_\alpha \right\rangle = \langle q\Psi_\alpha \rangle = q_\alpha. \tag{63}$$

The determination of the stochastic modes of $F^q(\cdot;\xi)$ and $F^E(\cdot;\xi)$ is more complex because these fluxes are nonlinear. Contrary to approaches that compute the Galerkin flux $f(u)$ in a non-intrusive way by a quadrature formula, we consider an approximation of the projection of the flux $F(\cdot;\xi)$ on $\mathcal{S}^{\mathrm{P}}$, denoted by $F^{\mathrm{P}}(\cdot;\xi)$, that we compute in a pseudo-spectral way

$$F(\cdot;\xi) \approx F^{\mathrm{P}}(\cdot;\xi) = \sum_{\alpha=0}^{\mathrm{P}} (f^{\mathrm{P}})_\alpha \Psi_\alpha(\xi). \tag{64}$$

The Galerkin flux $f(u)$ is therefore approximated as

$$f(u) \approx f^{\mathrm{P}}(u) = (f^{\mathrm{P}})_{\alpha=0,\ldots,\mathrm{P}}. \tag{65}$$

To this end, we rely on [6], which describes tools for accurate evaluations of polynomial and non-polynomial functions of variables represented by stochastic expansions. For instance, the components of the pressure $p = (\gamma-1)(E - 1/2\rho v^2)$ are computed in the following way. We first compute the expansion of $q^2(\xi)$ from the expansion of $q(\xi)$,

$$q^2(\xi) = \left(\sum_{\alpha=0}^{\mathrm{P}} q_\alpha \Psi_\alpha\right)\left(\sum_{\alpha=0}^{\mathrm{P}} q_\alpha \Psi_\alpha\right) = \sum_{\alpha,\beta=0}^{\mathrm{P}} q_\alpha q_\beta \Psi_\alpha \Psi_\beta. \tag{66}$$

Generally, $q^2 \notin \mathcal{S}^{\mathrm{P}}$ (its expansion possesses terms with degree $>$ No), and we approximate its expansion on $\mathcal{S}^{\mathrm{P}}$ as

$$q^2 \approx q * q = \sum_{\alpha=0}^{\mathrm{P}} (q*q)_\alpha \Psi_\alpha, \quad (q*q)_\alpha = \sum_{\beta,\delta=0}^{\mathrm{P}} q_\beta q_\delta \mathcal{M}_{\alpha\beta\delta}, \tag{67}$$

where we have denoted by $*$ the stochastic product in $\mathcal{S}^{\mathrm{P}}$ defined using the multiplication tensor $\mathcal{M}_{\alpha\beta\delta} \equiv \langle \Psi_\alpha \Psi_\beta \Psi_\delta \rangle$. This third-order tensor depends only on the stochastic basis, can be computed once and for all at the beginning of the simulation, and its sparse character in the stochastic space is exploited for its storage. The product between two stochastic expansions is the most basic operation for the treatment of nonlinearities and is used to define other nonlinear operations. For instance, the kinetic energy $\rho v^2 = q^2/\rho$ on $\mathcal{S}^{\mathrm{P}}$ is approximated as

$$\rho v^2 = q^2/\rho \approx (q*q) * 1/\rho, \tag{68}$$

where $q*q$ is defined by (67) and the approximation of $1/\rho$ is obtained from the resolution of a linear system obtained by setting $\rho * (1/\rho) = 1$ [6]. Finally, the approximation of the expansion of p on $\mathcal{S}^{\mathrm{P}}$ is

$$p \approx (\gamma - 1) * (E - (q*q) * (1/\rho)/2). \tag{69}$$

All in all, the approximation of the Galerkin flux amounts to the application of four stochastic products and a stochastic inversion. It should be stressed that the resulting flux is inexact, due to intermediate truncation errors. Nervertheless, for well resolved simulations, this estimate should be correct enough. The analysis of the impact of errors induced by pseudo-spectral approximations goes beyond the present scope; we refer to [6] for a general discussion.

Computation of the Galerkin Jacobian matrix. In view of the application of Roe's scheme, we need to compute the Galerkin Jacobian matrix $\nabla_u f(u) \in \mathbb{R}^{3(\mathrm{P}+1),3(\mathrm{P}+1)}$. As previously, we consider an approximation of the projection of $\nabla_U F(\cdot;\xi)$ on $\mathcal{S}^{\mathrm{P}}$, computed in a pseudo-spectral way with the tools described above, so that

$$\nabla_U F(\cdot;\xi) \approx \nabla_U F^{\mathrm{P}}(\cdot;\xi) = \sum_{\alpha=0}^{\mathrm{P}} (\nabla_u f^{\mathrm{P}})_\alpha \Psi_\alpha(\xi), \tag{70}$$

and the Galerkin Jacobian matrix $\nabla_u f(u)$ is approximated as

$$\begin{aligned} \nabla_u f(u) \approx \nabla_u f^{\mathrm{P}}(u) &= \left\langle \left(\nabla_U F^{\mathrm{P}}(U^{\mathrm{P}};\cdot)\right)_{ij} \Psi_\alpha \Psi_\beta \right\rangle_{0\le\alpha,\beta\le\mathrm{P},1\le i,j\le 3} \\ &\equiv \left(\sum_{\delta=0}^{\mathrm{P}} \left((\nabla_u f^{\mathrm{P}})_\delta\right)_{ij} \mathcal{M}_{\alpha\beta\delta} \right)_{0\le\alpha,\beta\le\mathrm{P},1\le i,j\le 3}. \end{aligned} \tag{71}$$

For instance, $(\nabla_u f^{\mathrm{P}}(u))_{\alpha\beta,12} = \delta_{\alpha\beta}$, and $(\nabla_u f^{\mathrm{P}}(u))_{\alpha\beta,33} = \sum_{\delta=0}^{\mathrm{P}} (\gamma * v)_\delta \mathcal{M}_{\alpha\beta\delta}$, $\forall \alpha,\beta = 0,\ldots,\mathrm{P}$. In terms of computational complexity, this approach requires nine stochastic products and a stochastic inversion. The summations can be conveniently optimized by exploiting the sparse structure of the multiplication tensor.

Computation of $\nabla_u f(u_{LR}^{\mathrm{Roe}})$ and its absolute value. As before, we rely on pseudo-spectral approximations to compute the stochastic modes of the Roe state's components defined by (59). A nonlinear system is solved with Newton's method to approximate the square root of the density in S^{P} by setting $\sqrt{\rho} * \sqrt{\rho} = \rho$. Finally, the absolute value of $\nabla_u f(u_{LR}^{\mathrm{Roe}})$ is computed as described in sections 4.2 and 4.3, using the stochastic eigenvalues of $\nabla_U F(U_{LR}^{\mathrm{Roe,P}}, \xi)$ at Gauss points in each stochastic element.

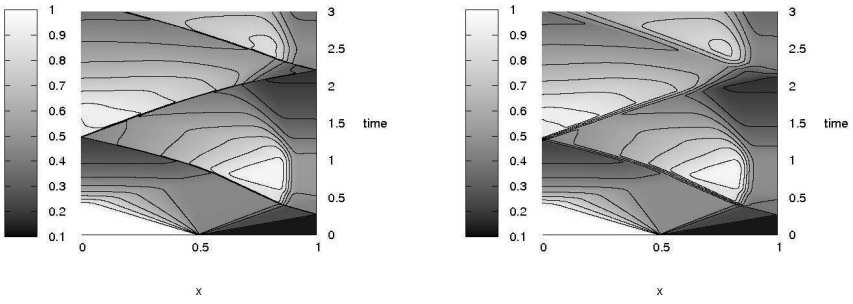

Figure 14: Space-time diagram of the deterministic density (left) and the expected density computed with parameters No = 2 and Nr = 3 (right).

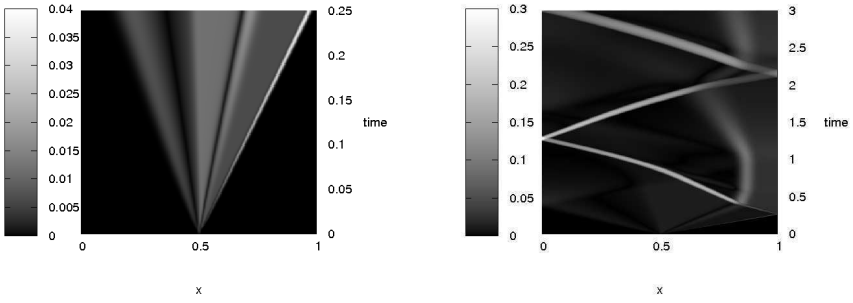

Figure 15: Space-time diagram of the standard deviations in the density for early (left) and longer times (right) computed with parameters No = 2 and Nr = 3. Different color scales are used.

5.3.3. Results analysis

In this section we present and analyze the results for the shock tube problem with uncertainty in the adiabatic coefficient. We make first a general analysis of the results, taking No = 2 and Nr = 3 as stochastic discretization parameters, so that the dimension of the stochastic space is 24.

In the deterministic case and for the initial condition (57) for a certain realization of $\gamma(\xi)$, a shock wave generated at the discontinuity travels to the right with velocity $v + c$, while a slower rarefaction fan travels to the left with velocity $v - c$, and a contact discontinuity wave travels to the right with velocity v. When the waves reach the solid wall, they are reflected inside the domain and so propagate toward each other, merge, and interact. When the waves have crossed each other, they continue to propagate up to the point where they again reflect on a wall, and so on.

Here, the uncertain sound velocity will affect the propagation velocity of the shock wave, contact discontinuity, and rarefaction fan. Solutions for different realizations of $\gamma(\xi)$ exhibit similar patterns as in the deterministic case, but with different slopes for the shock, contact discontinuity, and rarefaction fan in the space-time diagram. This is verified in Figure 14 where the density in the deterministic case and its expectation in the stochastic case are plotted. The spreading of the location of both the shock and the contact discontinuity when time increases is clearly visible, while for the rarefaction fan, which is already

smooth in the deterministic case, the impact of the uncertain sound velocity is less pronounced.

The impact of the uncertainty can also be appreciated from the standard deviations of the density, reported in Figure 15 for early and longer times. The highest values of the standard deviations are observed along the path of the shock wave, the maximum values corresponding to times at which the shock wave reflects on the tube walls. For early times ($t \leq 0.25$), uncertainty is present only in areas where the shocks can depend on the sound velocity in the prescribed uncertainty range. The first process leading to larger uncertainty levels is the shock-wall interaction since the arrival of the shock at a wall causes an abrupt increase of the density over a short time interval. The uncertainty in the arrival time of the shock wave therefore induces a large variability in the solution. The second process leading to larger uncertainty levels is the interaction between the uncertain shock, contact discontinuity, and rarefaction fan.

To assess the validity of the stochastic expansion, we show in Figure 16 a reconstruction of the stochastic density $\rho(x,t,\xi)$ at selected times. The discontinuity in $\rho(x,\cdot,\xi)$ is initially in the x-direction. As time increases, the density becomes discontinuous in both x- and ξ-directions since the stochastic wave propagates with an uncertain velocity. In the (x,ξ)-plane, the discontinuity becomes more and more oblique reflecting a monotonic dependence of the shock velocity on ξ. For points (x,ξ) not too close to the discontinuity, the solution is smooth and appears to be accurately approximated by the stochastic expansion. In the neighborhood of the discontinuity, the solution exhibits small unphysical oscillations that are triggered by the well-known Gibbs phenomenon so that the density takes values slightly outside its expected range. Such oscillations appear to be caused by an unsufficient stochastic resolution and can be reduced by increasing the resolution level and/or the polynomial order of the stochastic approximation. This is illustrated in Figures 17 and 18, which show the convergence of the density field as the value of No or Nr is increased. Oscillations become smaller as the level of stochastic resolution increases.

To complete the discussion, we provide a brief estimate of the computational efficiency of the numerical method for the Euler problem with random γ. We show in Table 1 the evolution of the computational times for different stochastic discretizations. CPU times (T_{CPU}) are reported for an integration of the Euler equations up to $t = 3$ on a fixed grid having $\mathrm{Nc} = 250$ cells, and are normalized by the computational time using $\mathrm{No} = \mathrm{Nr} = 0$, *i.e.* for the deterministic problem. Since the time step for the integration is based on a fixed CFL, it also depends on the stochastic discretization: the measured times correspond to different numbers of iterations performed. However, we observed roughly 0.5% variability in the number of time iterations between the most and least refined simulations such that the CPU times can also be interpreted as times to perform a fixed number of iterations.

Inspection of T_{CPU} in Table 1 shows a linear scaling with the number 2^{Nr} of stochastic elements for fixed polynomial order No. This scaling was expected and achieved thanks to the decoupling of the Galerkin problems over the stochastic elements for the projection on the SE basis. This linear scaling is expected to hold also for higher-dimensional problems ($\mathrm{N} > 1$), so in general we shall have $T_{CPU} \sim \mathcal{O}(2^{\mathrm{Nr}})$ for uniform partitions of the stochastic domain.

For fixed resolution level Nr, the scaling of T_{CPU} with the dimension of $\mathcal{S}^{\mathrm{No,Nr}}$ is roughly linear at least for $\mathrm{No} \leq 4$, as shown in Table 1. There are two effects. Firstly, the spectral evaluation of the nonlinearities in the flux and Roe's states have a complexity (number of operation counts) that essentially scale with the number of non zero terms in the Galerkin multiplication tensor $\mathcal{M}_{\alpha\beta\delta}$, which itself increases exponentially with No. Secondly, as No increases, a higher degree d has to be used for the polynomial approximation of the upwind matrixes, with higher computational costs as a result. The second effect can be tempered, based on the numerical experiments on the Burgers equation, by limiting d to a low value; the present simulations actually used a definition $d+1 = min(9, 3(\mathrm{No}+1))$, since allowing for higher degree d for $\mathrm{No} \geq 3$ was found to have no significant effect on the solution. All in all, the complexity of the nonlinearity resolution appears to be the most limiting factor of the present method, and this effect is expected to be worse for problems with higher stochastic dimension N (see for instance [16]): this trend pleads for using multi-resolution schemes with low-order expansions for non-smooth stochastic problems.

	Nr = 2		Nr = 3		Nr = 4	
	T_{CPU}	$\dim \mathcal{S}^{\mathrm{Nr,No}}$	T_{CPU}	$\dim \mathcal{S}^{\mathrm{Nr,No}}$	T_{CPU}	$\dim \mathcal{S}^{\mathrm{Nr,No}}$
No = 0	4.0	(4)	8.1	(8)	16.1	(16)
No = 1	6.9	(8)	13.9	(16)	27.8	(32)
No = 2	11.8	(12)	23.2	(24)	46.5	(48)
No = 3	17.1	(16)	34.1	(32)	68.1	(64)
No = 4	24.8	(20)	49.3	(40)	98.0	(80)

Table 1: Normalized computational times T_{CPU} for different stochastic discretization parameters Nr and No.

6. Conclusion

In this paper we have investigated theoretically and numerically a fully intrusive multi-resolution scheme for stochastic hyperbolic systems of conservation laws, exhibiting discontinuities in both physical and stochastic spaces. The method is based on the Galerkin projection of the original stochastic problem on a space of piecewise polynomials and uses a Roe-type solver with upwind matrices that are efficiently computed by an original and fast method. Numerical tests on the stochastic Burgers and Euler equations in one spatial dimension and, respectively, in two and one stochastic dimensions indicate that the method is accurate and robust while maintaining moderate computational costs. Nevertheless, further savings in computational costs are necessary to explore problems with higher stochastic dimensions. To this purpose, adaptive stochastic mesh refinement methods are the focus of ongoing efforts. Furthermore, extension of Roe solvers to include for instance entropy correctors is under investigation. Finally, additional mathematical studies are still needed to consolidate the theoretical bases of the method.

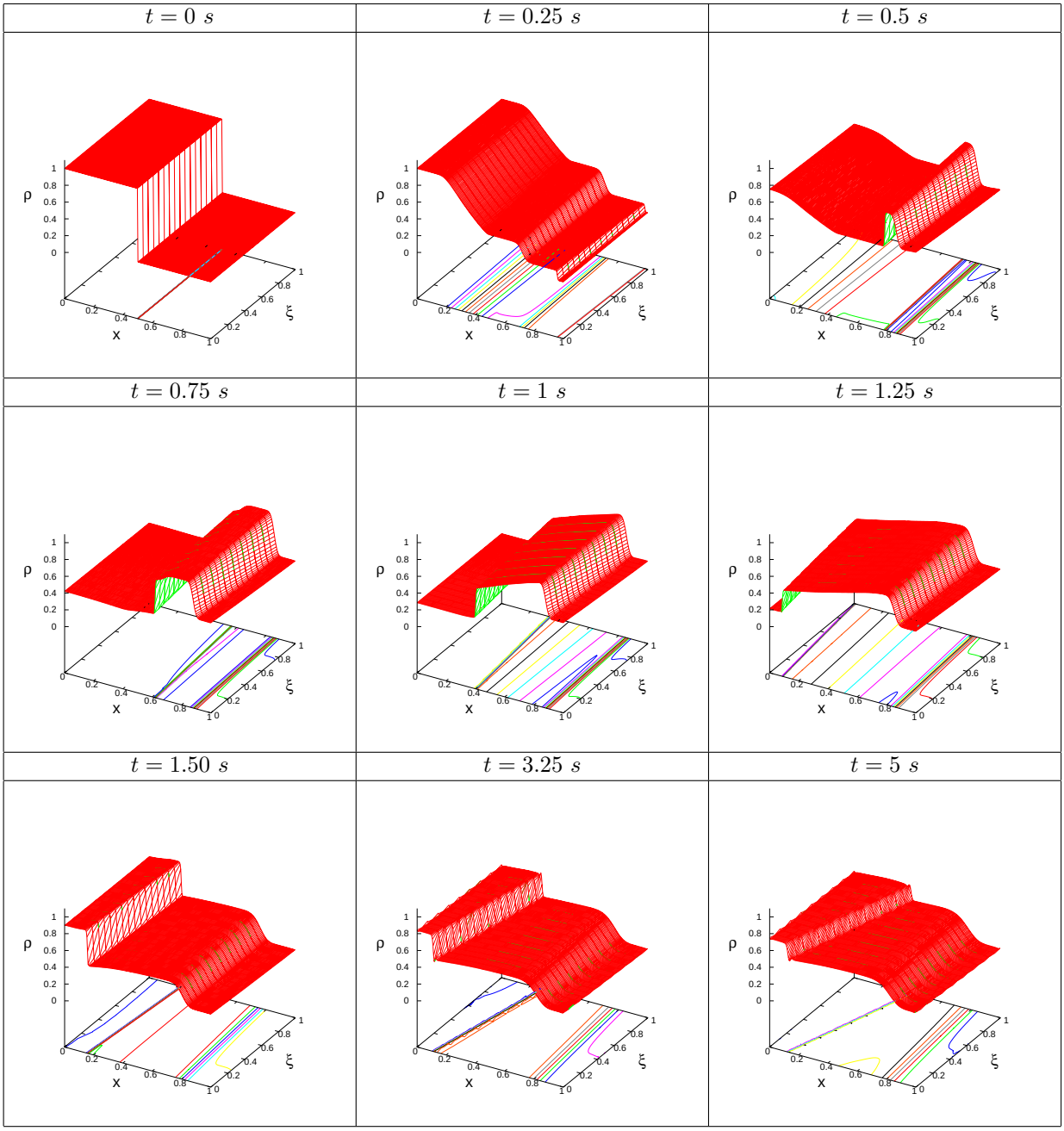

Figure 16: Reconstruction of the stochastic density $\rho(x, t; \xi)$ at selected times.

No $= 0$ et Nr $= 3$ ($\#\mathcal{S}^{\mathrm{No,Nr}} = 8$)	No $= 1$ et Nr $= 3$ ($\#\mathcal{S}^{\mathrm{No,Nr}} = 16$)
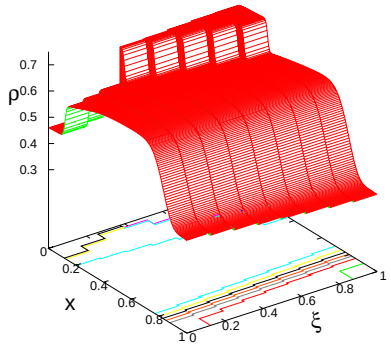	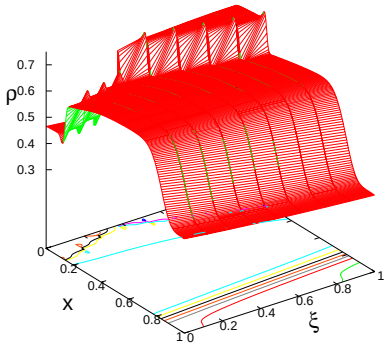
No $= 2$ et Nr $= 3$ ($\#\mathcal{S}^{\mathrm{No,Nr}} = 24$)	No $= 3$ et Nr $= 3$ ($\#\mathcal{S}^{\mathrm{No,Nr}} = 32$)
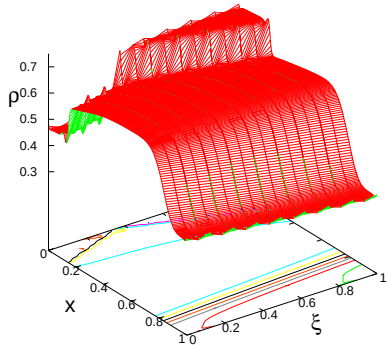	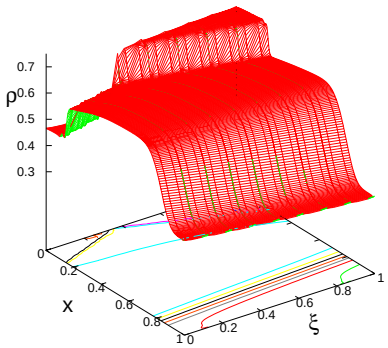

Figure 17: Convergence of the stochastic density $\rho(x, t; \xi)$ with No. Nr $= 3$, $t = 6.5$ s.

No $= 1$ et Nr $= 1$ ($\#\mathcal{S}^{\mathrm{No,Nr}} = 4$)	No $= 1$ et Nr $= 2$ ($\#\mathcal{S}^{\mathrm{No,Nr}} = 8$)
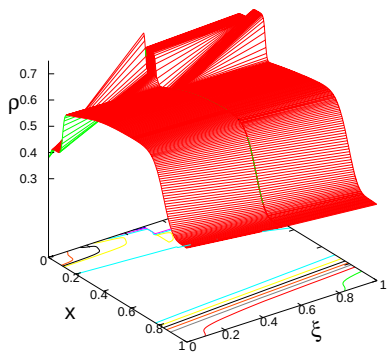	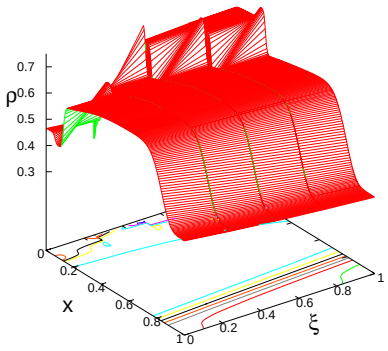
No $= 1$ et Nr $= 3$ ($\#\mathcal{S}^{\mathrm{No,Nr}} = 16$)	No $= 1$ et Nr $= 4$ ($\#\mathcal{S}^{\mathrm{No,Nr}} = 32$)
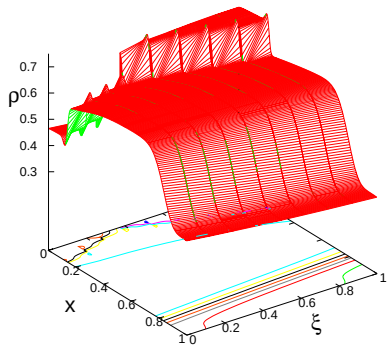	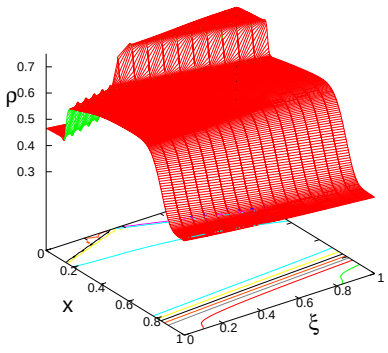

Figure 18: Convergence of the stochastic density $\rho(x, t; \xi)$ with Nr. No $= 1$, $t = 6.5$ s.

References

[1] R. Abgrall. A simple, flexible and generic deterministic approach to uncertainty quantifications in non linear problems: application to fluid flow problems. *Rapport de recherche INRIA*, 00325315, 2008.

[2] Ivo Babuška, Fabio Nobile, and Raúl Tempone. A stochastic collocation method for elliptic partial differential equations with random input data. *SIAM J. Numer. Anal.*, 45(3):1005–1034, 2007.

[3] Alexandre Joel Chorin. Gaussian fields and random flow. *J. Fluid Mech.*, 63:21–32, 1974.

[4] Manas K. Deb, Ivo M. Babuška, and J. Tinsley Oden. Solution of stochastic partial differential equations using Galerkin finite element techniques. *Comput. Methods Appl. Mech. Engrg.*, 190(48):6359–6372, 2001.

[5] B. Debusschere, H.N. Najm, A. Matta, O.M. Knio, R.G. Ghanem, and O.P. Le Maître. Protein Labeling Reactions in Electrochemical Microchannel Flow: Numerical Prediction and Uncertainty Propagation. *Physics of Fluids*, 15(8):2238–2250, 2003.

[6] Bert J. Debusschere, Habib N. Najm, Philippe P. Pébay, Omar M. Knio, Roger G. Ghanem, and Olivier P. Le Maître. Numerical challenges in the use of polynomial chaos representations for stochastic processes. *SIAM J. Sci. Comput.*, 26(2):698–719, 2004.

[7] Pierre Degond, Pierre-François Peyrard, Giovanni Russo, and Philippe Villedieu. Polynomial upwind schemes for hyperbolic systems. *C. R. Acad. Sci. Paris Sér. I Math.*, 328(6):479–483, 1999.

[8] Jasmine Foo, Xiaoliang Wan, and George Em Karniadakis. The multi-element probabilistic collocation method (ME-PCM): error analysis and applications. *J. Comput. Phys.*, 227(22):9572–9595, 2008.

[9] Baskar Ganapathysubramanian and Nicholas Zabaras. Sparse grid collocation schemes for stochastic natural convection problems. *J. Comput. Phys.*, 225(1):652–685, 2007.

[10] L. Ge, K.F. Cheung, and M.H. Kobayashi. Stochastic Solution for Uncertainty Propagation in Nonlinear Shallow-Water Equations. *Journal of Hydraulic Engineering*, Decembre 2008:1732–1743, 2008.

[11] Roger G. Ghanem and Pol D. Spanos. *Stochastic finite elements: a spectral approach*. Dover, 2003.

[12] Edwige Godlewski and Pierre-Arnaud Raviart. *Numerical approximation of hyperbolic systems of conservation laws*, volume 118 of *Applied Mathematical Sciences*. Springer-Verlag, New York, 1996.

[13] David Gottlieb and Dongbin Xiu. Galerkin method for wave equations with uncertain coefficients. *Commun. Comput. Phys.*, 3(2):505–518, 2008.

[14] A. Keese and H.G. Matthies. Numerical methods and Smolyak quadrature for nonlinear stochastic partial differential equations. Technical report, Institute of Scientific Computing TU Braunschweig Brunswick, 2003.

[15] O. M. Knio and O. P. Le Maître. Uncertainty propagation in CFD using polynomial chaos decomposition. *Fluid Dynam. Res.*, 38(9):616–640, 2006.

[16] O. Le Maître. A Newton method for the resolution of steady stochastic Navier-Stokes equations. *Comput Fluids*, 2009. in press, doi:10.1016/j.compfluid.2009.01.001.

[17] O. P. Le Maître, O. M. Knio, H. N. Najm, and R. G. Ghanem. Uncertainty propagation using Wiener-Haar expansions. *J. Comput. Phys.*, 197(1):28–57, 2004.

[18] O. P. Le Maître, H. N. Najm, R. G. Ghanem, and O. M. Knio. Multi-resolution analysis of Wiener-type uncertainty propagation schemes. *J. Comput. Phys.*, 197(2):502–531, 2004.

[19] O. P. Le Maître, H. N. Najm, P. P. Pébay, R. G. Ghanem, and O. M. Knio. Multi-resolution-analysis scheme for uncertainty quantification in chemical systems. *SIAM J. Sci. Comput.*, 29(2):864–889, 2007.

[20] Olivier Le Maître, M. T. Reagan, B. Debusschere, H. N. Najm, R. G. Ghanem, and O. M. Knio. Natural convection in a closed cavity under stochastic non-Boussinesq conditions. *SIAM J. Sci. Comput.*, 26(2):375–394, 2004.

[21] Olivier P. Le Maître, Omar M. Knio, Habib N. Najm, and Roger G. Ghanem. A stochastic projection method for fluid flow. I. Basic formulation. *J. Comput. Phys.*, 173(2):481–511, 2001.

[22] Olivier P. Le Maître, Matthew T. Reagan, Habib N. Najm, Roger G. Ghanem, and Omar M. Knio. A stochastic projection method for fluid flow. II. Random process. *J. Comput. Phys.*, 181(1):9–44, 2002.

[23] G. Lin, C.-H. Su, and G. E. Karniadakis. Predicting shock dynamics in the presence of uncertainties. *J. Comput. Phys.*, 217(1):260–276, 2006.

[24] G. Lin, C.-H. Su, and G. E. Karniadakis. Stochastic modeling of random roughness in shock scattering problems: theory and simulations. *Comput. Methods Appl. Mech. Engrg.*, 197(43-44):3420–3434, 2008.

[25] L. Mathelin and M. Hussaini. A stochastic collocation algorithm for uncertainty analysis. Technical Report NASA/CR-2003-212153, NASA Langley Research Center, 2003.

[26] Lionel Mathelin, M. Yousuff Hussaini, and Thomas A. Zang. Stochastic approaches to uncertainty quantification in CFD simulations. *Numer. Algorithms*, 38(1-3):209–236, 2005.

[27] H.N. Najm, B.J. Debussechre, Y.M. Marzouk, S. Widmer, and O.P. Le Maître. Uncertainty quantification in chemical systems. *Int. J. Numer. Meth. Engng*, 2009. in press, doi: 10.1002/nme.2551.

[28] Michaël Ndjinga. Computing the matrix sign and absolute value functions. *C. R. Math. Acad. Sci. Paris*, 346(1-2):119–124, 2008.

[29] F. Nobile, R. Tempone, and C. G. Webster. A sparse grid stochastic collocation method for partial differential equations with random input data. *SIAM J. Numer. Anal.*, 46(5):2309–2345, 2008.

[30] G. Poette, B. Després, and D. Lucor. Uncertainty quantification for systems of conservation laws. *J. Comput. Phys.*, 228(7):2443–2467, 2009.

[31] M.T. Reagan, H.N. Najm, R.G. Ghanem, and O.M. Knio. Uncertainty quantification in reacting flow simulations through non-intrusive spectral projection. *Combustion and Flame*, 132:545–555, 2003.

[32] Eleuterio F. Toro. *Riemann solvers and numerical methods for fluid dynamics*. Springer-Verlag, Berlin, second edition, 1999. A practical introduction.

[33] Xiaoliang Wan and George Em Karniadakis. Multi-element generalized polynomial chaos for arbitrary probability measures. *SIAM J. Sci. Comput.*, 28(3):901–928 (electronic), 2006.

[34] Norbert Wiener. The Homogeneous Chaos. *Amer. J. Math.*, 60(4):897–936, 1938.

[35] Dongbin Xiu and Jan S. Hesthaven. High-order collocation methods for differential equations with random inputs. *SIAM J. Sci. Comput.*, 27(3):1118–1139, 2005.

[36] Dongbin Xiu and George Em Karniadakis. The Wiener-Askey polynomial chaos for stochastic differential equations. *SIAM J. Sci. Comput.*, 24(2):619–644 (electronic), 2002.